

**FABRICATION OF A NOVEL MAGNETIC NANOCOMPOSITE  
BASED ON 3D CROSSLINKED POLY(ACRYLIC ACID) AND  
CARBOXYLATED CELLULOSE NANOCRYSTAL**

A thesis submitted in partial fulfillment of the requirement for  
the degree of M.Sc. in chemistry

**SUBMITTED BY**

**ABINASH CHANDRA ROY  
STUDENT ID: 1014032711  
SESSION: OCTOBER 2014**



**Chemistry Materials Laboratory  
Department of Chemistry  
Bangladesh University of Engineering and Technology (BUET)  
Dhaka-1000, Bangladesh**

**February 2017**

## DECLARATION BY THE CANDIDATE

I do hereby declare that this thesis work, entitled “**FABRICATION OF A NOVEL MAGNETIC NANOCOMPOSITE BASED ON 3D CROSSLINKED POLY(ACRYLIC ACID) AND CARBOXYLATED CELLULOSE NANOCRYSTAL**” submitted in partial fulfillment for the requirement of M.Sc. Degree in Chemistry to the Department of Chemistry, Bangladesh University of Engineering and Technology (BUET) in February 2017, is genuine work done by me under the supervision of Dr. Md. Shafiul Azam, Assistant Professor, Department of Chemistry, Bangladesh University of Engineering and Technology (BUET). The thesis or part of it has not been submitted before in any degree or diploma.



.....  
**(Abinash Chandra Roy)**

M.Sc. student

Department of Chemistry

Bangladesh University of Engineering and Technology (BUET)

Dhaka, Bangladesh

## CERTIFICATE

This is to certify that this thesis work entitled “**FABRICATION OF A NOVEL MAGNETIC NANOCOMPOSITE BASED ON 3D CROSSLINKED POLY(ACRYLIC ACID) AND CARBOXYLATED CELLULOSE NANOCRYSTAL**” submitted by Abinash Chandra Roy, Student ID: 1014032711, to the Department of Chemistry, Bangladesh University of Engineering and Technology (BUET) in partial fulfillment for the requirement of M.Sc. in Chemistry in February 2017 is based on his original research and investigation carried out under my guidance and supervision.

Supervisor:



.....  
**Dr. Md. Shaful Azam**

Assistant Professor

Department of Chemistry

Bangladesh University of Engineering & Technology (BUET)

Dhaka, Bangladesh

**Bangladesh University of Engineering and Technology, Dhaka**  
**Department of Chemistry**



**Certification of Thesis**

**A thesis on**

**FABRICATION OF A NOVEL MAGNETIC NANOCOMPOSITE BASED ON 3D  
CROSSLINKED POLY(ACRYLIC ACID) AND CARBOXYLATED CELLULOSE  
NANOCRYSTAL**

**BY**

**Abinash Chandra Roy**

has been accepted as satisfactory in partial fulfillment of the requirements for the degree of Master of Science (M.Sc.) in Chemistry and certify that the student has demonstrated a satisfactory knowledge of the field covered by this thesis in an oral examination held on February 13, 2017.

**Board of Examiners**

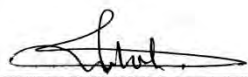
**1. Dr. Md. Shafiul Azam**

Assistant Professor  
Department of Chemistry  
BUET, Dhaka

  
13.02.17  
Supervisor & Chairman

**2. Dr. Md. Rafique Ullah**

Professor & Head  
Department of Chemistry  
BUET, Dhaka

  
Member (Ex-officio) 13/02/2017.

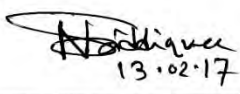
**3. Dr. Md. Shakhawat Hossain Firoz**

Associate Professor  
Department of Chemistry  
BUET, Dhaka

  
13-02-17  
Member

**4. Dr. Muhammad Nurunnabi Siddiquee**

Associate Professor  
Department of Chemical Engineering &  
Polymer Science  
Shahjalal University of Science and  
Technology, Sylhet

  
13.02.17  
Member (External)

*Dedicated to*  
*My Beloved Parents*  
*&*  
*Honorable supervisor*

# Acknowledgement

At the very beginning, I humbly acknowledge my deepest gratitude to the almighty, the most gracious, benevolent and merciful creator for his infinite mercy bestowed on me in carrying out the research work presented in the dissertation.

It is a great pleasure for me to acknowledge my deepest sense of gratitude, sincere, appreciation, heartfelt indebtedness and solemn regards to my reverend teacher and supervisor Dr. Md. Shafiul Azam, Assistant Professor, Department of Chemistry, Bangladesh University of Engineering and Technology (BUET), for his kind supervision, indispensable guidance, valuable and constructive suggestions, liberal help and continuous encouragement during the whole period. It is obvious that his attributive contribution and efforts have greatly shaped me into what I am today. In fact, I am quite lucky to be a part of his ambitious research team.

It is my great honor to convey my sincere gratitude to my respected teacher Professor Dr. Md. Rafique Ullah, honorable Head of the Department of Chemistry, BUET for giving me his wonderful support to move through the academic processes during this M.Sc. program.

I would like to convey my deepest gratitude to Professor Dr. Md. Nazrul Islam, Dr. Md. Shakhawat Hossain Firoz, and Md. Abu Hasan Howlader, Department of Chemistry, BUET, for their valuable suggestions, appreciated comments, guidance and help during the research period.

I am thankful to all other respected teachers of the Department of Chemistry, BUET, for their time to time support. I would also like to thank all of the officers and staffs of the Department of Chemistry, BUET for their continuous help during my study period.

I am highly thankful to Professor Dr. Hongbo Zeng, University of Alberta, Canada, for the characterization of our samples using X-ray Photoelectron Spectroscopy (XPS) technique during my research.

I am highly grateful to all members of the board of examiners for their valuable suggestions and appreciated comments.

I am thankful to my dear colleagues Md. Shafiqul Islam, Labiba Bushra, Salma Sultana, Shuvo Das, for their friendly cooperation and lovely encouragement throughout my research period. Special thanks to Md. Jahangir Hossen, Technical Officer, Bangladesh University of Textiles (BUTEX) for his continuous help during the research.

I am also thankful to other fellows of Chemistry Materials Laboratory for their cooperation during the research period.

I am grateful to the authority of BUET and The World Academy of Sciences (TWAS) for providing financial support for this research work.

Finally, I would like to express my heartfelt indebtedness and profound gratitude to my beloved father, mother and all of my family members for their continuous inspiration and immeasurable sacrifices throughout the period of my study.

February, 2017

Abinash Chandra Roy

# Abstract

In this research, synthesis and characterization of a new magnetic nanocomposite based on 3D crosslinker and carboxylated cellulose nanocrystal have been carried out. The magnetic particles are directly linked with the polymer chain by strong covalent bond. A highly reactive site containing 3D crosslinker was introduced for the linking between the magnetic particles and the polymer chain. Magnetic iron oxide nanoparticle (MION) was synthesized via co-precipitation method and then coated with silica. This silica coated MION was further functionalized by amino group followed by incorporation of acrylic group. The synthesized product acted as 3D crosslinker with the reactive acrylic group on the surface. The 3D crosslinking achieved by using this crosslinker made the polymers more robust due to the presence of enormous number of active sites on a single component. The dispersive property of the nanocomposite was increased by incorporation of highly dispersive carboxylated cellulose nanocrystal which was extracted from sawdust by acid hydrolysis process followed by 2, 2, 6, 6-tetramethylpiperidin-1-oxyl (TEMPO)-mediated oxidation. The synthesized nanocomposite was characterized by x-ray photoelectron spectroscopy (XPS), x-ray diffraction (XRD), energy dispersive x-ray (EDX), field emission scanning electron microscopy (FE-SEM), thermogravimetric analysis (TGA) and fourier transform infrared (FTIR) analysis. From FE-SEM study it was found that the size of the particle of the nanocomposite was 60-90nm. The chemical functionalities were characterized by XPS and FTIR which was relevant to the corresponding components. TGA study showed the magnetic nanocomposite was highly thermo stable.



# Contents

1 Introduction.....	1
1.1 General remarks.....	2
1.2 Nanocomposite.....	2
1.2.1 Ceramic matrix nanocomposite.....	3
1.2.2 Metal matrix nanocomposite.....	3
1.2.3 Polymer nanocomposite.....	3
1.3 Nanofiller.....	4
1.3.1 Nanoclay.....	5
1.3.2 Nano-oxide.....	5
1.3.3 Metallic nanoparticles.....	6
1.3.4 Nanocellulosic materials.....	6
1.4 Cellulose.....	7
1.4.1 Cellulose nanocrystal (CNC).....	8
1.4.2 Carboxylated cellulose nanocrystal (CCN).....	9
1.5 Crosslinker.....	11
1.5.1 Linear crosslinker.....	11
1.5.2 Planar (2D) crosslinker.....	12
1.5.3 Three dimensional crosslinker.....	12
1.6 Magnetically responsive polymer nanocomposite .....	13
1.7 Magnetic nanoparticles.....	13
1.7.1 Co-precipitation method.....	14
1.7.2 Surface modification of iron oxide nanoparticles.....	15
1.8 Research goal.....	15
References .....	16
2. Experimental.....	25
2.1 Materials and instruments.....	26
2.2 Chemicals and reagents.....	26
2.3 Instruments.....	27
2.2 Fabrication of a novel magnetic nanocomposite.....	27
2.2.1 Extraction of cellulose nanocrystal.....	27
2.2.2 Synthesis of carboxylated cellulose nanocrystal.....	28
2.2.3 Synthesis of acrylated magnetic iron oxide nanoparticles.....	29

2.2.4 Synthesis of nanocomposite.....	30
2.3 Conductometric titration.....	31
2.4 Fourier transform infrared analysis (FTIR).....	31
2.5 Field emission scanning electron microscopy (FE-SEM).....	31
2.6 Energy dispersive x-ray (EDX).....	32
2.7 X-ray diffraction (XRD).....	32
2.8 X-ray photoelectron spectroscopy (XPS).....	32
2.9 Thermogravimetric analysis (TGA).....	33
References.....	34
3 Results and Discussion.....	35
3.1 Fabrication of magnetic nanocomposite.....	36
3.1.1 Synthesis of carboxylated cellulose nanocrystal (CCN).....	36
3.1.2 Synthesis of 3D crosslinker.....	37
3.1.3 Nanocomposite synthesis.....	38
3.2 Magnetic test of nanocomposite.....	41
3.3 Functional group analysis using FTIR.....	41
3.4 X-ray photoelectron spectroscopy (XPS) analysis.....	44
3.4.1 High resolution C1s spectra.....	45
3.4.2 High resolution N1s spectra.....	47
3.5 X-ray diffraction analysis (XRD).....	47
3.6 Surface morphology analysis using FE-SEM.....	49
3.7 Elemental analysis using EDX.....	52
3.8 Thermogravimetric analysis.....	56
3.9 Conclusion.....	58
References.....	59

**List of figures:**

Figure 1.1 Typical structure of cellulose .....	7
Figure 1.2 Degradation of amorphous region of cellulose by sulfuric acid.....	9
Figure 1.3 Cross sectional representation of cellulose nanocrystal indicating the occurrence of the surface TEMPO mediated oxidation of available hydroxyl groups.....	10
Figure 1.4 Synthesis of nanocomposite using 1D crosslinker.....	11
Figure 1.5 Synthesis of nanocomposite using 2D crosslinker.....	12

Figure 1.6 Synthesis of nanocomposite using 3D crosslinker.....	13
Figure 2.1 Schematic representation of extraction of CNC from sawdust.....	28
Figure 2.2 Schematic representation of carboxylated cellulose nanocrystal.....	29
Figure 3.1 Mechanism of TEMPO mediated oxidation (a) initial formation of oxidant from TEMPO radical (b) catalytic cycle of TEMPO oxidation.....	37
Figure 3.2 Schematic representation of 3D crosslinker synthesis.....	38
Figure 3.3 Schematic representation of nanocomposite synthesis.....	39
Figure 3.4 Different ratio of CCN, 3D crosslinker and acrylic acid in nanocomposite.....	40
Figure 3.5 Magnetic test of synthesized nanocomposite.....	41
Figure 3.6 FTIR spectra of CNC, CCN and nanocomposite.....	42
Figure 3.7 FTIR spectra of Fe <sub>3</sub> O <sub>4</sub> , silica coated MION, aminated MION and acrylated MION.....	43
Figure 3.8 Widescan spectra of aminated MION, acrylated MION and nanocomposite.....	44
Figure 3.9 High resolution C1s spectra of aminated MION, acrylated MION and nanocomposite.....	45
Figure 3.10 High resolution N1s spectra of aminated MION, acrylated MION and nanocomposite.....	47
Figure 3.11 XRD spectra of Fe <sub>3</sub> O <sub>4</sub> and nanocomposite.....	48
Figure 3.12 FE-SEM image of CNC (A) Resolution x 50,000 (B) Resolution x 100,000.....	49
Figure 3.13 FE-SEM image of CCN (A) Resolution x 50,000 (B) Resolution x 100,000.....	50
Figure 3.14 FE-SEM image of magnetic iron oxide nanoparticle (MION) (A) Resolution x 100,000 (B) Resolution x 150,000.....	50
Figure 3.15 FE-SEM image of silica coated (MION) (A) Resolution x 50,000 (B) Resolution x 100,000.....	51
Figure 3.16 FE-SEM image of acrylated MION (A) Resolution x 100,000 (B) Resolution x 150,000.....	51
Figure 3.17 FE-SEM image of nanocomposite (A) Resolution x 100,000 (B) Resolution x 150,000.....	52
Figure 3.18 EDX spectra of (A) Fe <sub>3</sub> O <sub>4</sub> (MION) and (B) silica coated MION.....	53
Figure 3.19 EDX spectra of (C) acrylated MION and (D) CNC.....	54
Figure 3.20 EDX spectra of (E) CCN and (F) nanocomposite.....	55
Figure 3.21 TGA curves of CCN, acrylated MION, composite without CCN	

and nanocomposite.....56

**List of tables:**

Table 3.1 Characteristic IR bands of CNC, CCN, and nanocomposite.....42  
Table 3.2 Elemental composition of magnetic and cellulosic compound.....52

# Chapter 1

## Introduction

## 1.1 General remarks

Composite materials have a long history. As early as 3000 B.C. the ancient Egyptians embedded straw in their mud bricks in order to control shrinkage cracks and improve the tensile strength. Since then many more new composite materials have been invented till now with the blends of different properties. A new dimension added to the field of composite material when the nanomaterials are invented. Nanomaterials are the cornerstones of nanoscience and nanotechnology. The transition from microparticles to nanoparticles gains remarkable changes in optical, electrical, mechanical and other physical properties. Generally, materials which have at least one dimension in 1-100 nm are called nanomaterials. Materials having one dimension in nanometer range are layers such as thin films or surface coatings. On the other hand, materials having two dimensions in nanometer range are nanotubes or nanowires and three dimensions in nanoscale are called nanoparticles. Nanomaterials added with composite show dramatic changes in physical as well as chemical properties. In 1998, Chemistry in Britain published an article titled 'Nano sandwiches', stating, 'Nature is a master chemist with incredible talent'. Using natural reagents and polymers such as carbohydrates, lipids, and proteins, nature makes strong composites such as bones, shells, and wood. In the early of 1990s, Toyota central research laboratories in Japan reported work on a nylon-6 nanocomposite, for which a very small amount of nanofiller loading resulted in a prominent improvement of thermal and mechanical properties. By changing nanofiller or matrices different types of nanocomposite are produced with the demand of current situation.

## 1.2 Nanocomposite

Nanocomposite is a composite or multiphase solid material in which at least one of the phases shows dimensions in the nanometer range [1]. Normally nanocomposite consists of continuous phase and nanofiller or reinforcing phase. The continuous phase may be of polymer, ceramic or metal and the nanofiller may be of nanoparticles, sheets or fibers. Nanocomposites differ from conventional composite materials because of exceptionally high surface to volume ratio of the nanofiller. The mechanical, electrical, thermal, optical, electrochemical and catalytic properties of the nanocomposites change noticeably from that of the component materials. Nanocomposites are widely used in environment protection [2], drug delivery system [3, 4], electronic devices [5], packing materials and so on.

### **1.2.1 Ceramic matrix nanocomposite**

In this class of composites the continuous phase is ceramic, i.e. a chemical compound from the group of oxides, nitrides, borides, silicides, carbides etc. and the dispersed phase is mainly metallic component. Ceramic is brittle in nature. By adding nanofiller into ceramic a noticeable change in physical property is found. Over the past half century ceramics have received significant attention due to its application as structural materials under conditions of high loading rates and high temperature. Titanium nitride (TiN), titanium carbide (TiC), chromium nitride (CrN), diamondlike carbon (DLC), tungsten carbide/carbon (WC/C) are some of the important ceramic materials used in coating applications [6]. Hauert and Patscheider reported that with these coatings, the toughness, thermal stability and environmental compatibility of the composite materials were also improved [7].

### **1.2.2 Metal matrix nanocomposite**

Metal matrix nanocomposites are metals reinforced with other metal, ceramic or organic compounds. They are made by dispersing the reinforcements in the metal matrix. Reinforcements should be stable and non reactive at working temperature. The most commonly used reinforcements are silicon carbide (SiC), aluminum oxide ( $Al_2O_3$ ), carbon nanotube, etc. Metallic composites containing nanoparticles could offer distinct advantages due to the inherent high temperature stability, high strength and modulus, thermal and electrical conductivity of the metal matrix nanocomposites [8, 9]. Aluminum and its alloys have attracted most attention as base metal in metal matrix composites due to their wide range of application in aircraft, aerospace, automobiles and different industries [10]. SiC reinforcement increases the tensile strength, hardness and density of the composite materials [11]. Magnesium alloys are commonly used in structural applications due to low cost, easy handling, good strength and ductility, and resistance to atmospheric corrosion [12].

### **1.2.3 Polymer nanocomposite**

Composite materials in which the continuous phase is the polymer and the dispersed phase is nanofiller are called polymer nanocomposites. Polymers consisting from small monomer size have extra benefits because the polymer chains contain many more functional groups in comparatively small area. As a result, it can easily interact with many more substrate or waste ingredients. Some polymers are pH sensitive. Polymers activity may change in acidic or basic

medium by changing pH due to the pH sensitivity of the polymer and hence polymer composites are widely used in various purposes. The use of biocompatible polymer is increasing day by day as they are environmental friendly. This new class of composite materials has become great attention worldwide due to their improved mechanical and physical properties as well as biocompatibility. This nanocomposite has added advantage of lower density and ease of processability. In polymer nanocomposites, the filler has at least one dimension in the nanometer scale and its nanoscale dispersion within the polymer matrix leads to the tremendous interfacial contacts between the polymer and the filler. A wide variety of polymer matrices include polyacrylates, poly(acrylic acid), poly(acrylonitrile), polystyrene, poly(vinyl pyridine), polyacrylamide, poly(N-isopropylacrylamide), poly(tetrafluoro ethylene), poly(n-vinyl pyrrolidone), poly(vinyl pyrrolidinone), poly(vinyl pyridine), poly(ethylene glycol), poly(ethylene vinyl alcohol), poly(vinylidene fluoride), poly(p-phenylenevinylene), poly(benzoxazole), poly(styrene-co-acrylonitrile), ethyl-vinyl-alcohol copolymers, polystyrene-polyisoprene diblock copolymers, polyamides, poly(ethylene terephthalate), poly(trimethylene terephthalate), poly(butylene terephthalate), polycarbonates, poly(ethylene oxide), ethylene oxide copolymers, poly(ethylene imine), poly(dimethyl siloxane), polybutadienes, butadiene copolymers, epoxidized natural rubber, epoxy polymer resins, polyurethanes, polyurethane-urea, polyimides, polysulfone etc. are used in polymer nanocomposite [13-23]. Polymer nanocomposites are synthesized using template method, exfoliation-intercalation-in situ polymerization method and melt intercalation method. Polymer nanocomposites are used in almost all sectors from domestic to aerospace.

### **1.3 Nanofiller**

“Filler” is a form of a material that is embedded in a polymeric matrix to consist of composite materials. Generally fillers are incorporated in the composite materials in order to improve or add various properties, e.g., mechanical, thermal, optical, dispersive, electric, magnetic, etc. Chemical structure and amount of the fillers are important factors for the determination of the properties of the composites. The shape, size, and state of dispersion of the fillers are included as morphological factor. If the filler size is less than 100 nm in one, two or three dimension is called nanofiller. Nanofillers can be distinguished from the larger fillers due to large surface area and unique nanometric size. Nanofillers show better reinforcement for the nanocomposite production [24] and are usually incorporated on a



weight basis 1% to 10% for the nanocomposite development [25, 26]. The chemical compatibility between nanofiller and polymer plays a vital role in both the dispersion of particles in the matrix and the adhesion between these phases. Surface modification of the nanofillers is also important to control the dispersion in the matrix and interaction with the polymer phase [27]. Mobility, crystallinity and orientation of the polymer in the interfacial region largely depend on the nanofiller [28]. Large interfacial region with nanofiller implies a larger portion of the polymer matrix can be affected. Nanofillers belong to organic and inorganic in nature. For the fabrication of nanocomposite, nanofillers are synthesized in mainly two processes like in situ and ex situ process. In the in situ route, the formation of nanofiller is carried out inside the polymer matrix and in the ex situ process the preformed nanofillers are dispersed into the polymer matrix. The main advantage of the ex situ approach is that wider range of reaction condition can be used for the preparation of the nanofillers, which allow wider variety and property of the fillers.

### **1.3.1 Nanoclay**

Clay or nanoclay filled polymer nanocomposites represent a new class of materials, which have attracted much attention because of their excellent physical properties such as high dimensional stability, gas barrier performance, flame retardancy, and mechanical strength when compared to the pure polymer or conventional composites (micro and macro composites). In nanocomposites nanoclays are used because of its natural abundance and very high form factor. Two types of clays like natural or synthetic are used as nanoplate fillers. Various natural and synthetic nanoclays including Kaolinite, Smectite,(Talc, Mica, Mommorillonite), Sepiolite, Saponite, FluoroHectorite, Zeolite, Kenyaite, Magadiite, Kanemite, Ilerite, Silhydrite etc. are widely used as nanofiller in nanocomposite [29, 30]. They are normally shell shaped crystalline structure with nanometric thickness.

### **1.3.2 Nano-oxides**

The fabrication of nanocomposites or nanoarrays having special properties with respect to nano-oxide particles is an emerging field of nanotechnology. Nano-oxides exhibit unique physical and chemical properties due to their limited size and a high density of corner or edge surface sites. Size-induced structural distortions associated with changes in cell parameters have been observed, for example, in nanoparticles of  $Al_2O_3$ , NiO,  $Fe_2O_3$ ,  $ZrO_2$ ,  $MoO_3$ ,  $CeO_2$ ,  $Y_2O_3$ . Structural and electronic properties drive the physical and chemical properties of the

composites because of strong influence in the conductivity and chemical reactivity. As the particle size decreases, the increasing number of surface and interface atoms generates stress/strain and related structural perturbations. Interactions with the substrate on which the nanoparticles are supported can complicate the situation and induce structural perturbations or phases not seen for the bulk state of the oxide. Nano-oxides are high potential filler materials for the development of nanocomposite. Magnetic nano-oxides filled nanocomposites have special advantages for the removal of dyes, heavy metals etc. from the wastewater due to their easy separation. Hence magnetic nanocomposites play a vital role in nanotechnology. Nano-oxides like ZnO, CuO, TiO<sub>2</sub> etc. show antibacterial activity and hence the application of single oxide and multi oxide based nanocomposite increasing day by day. Nano-oxides like SiO<sub>2</sub> [31], TiO<sub>2</sub> [32], ZnO [33, 34], Al<sub>2</sub>O<sub>3</sub> [35], Fe<sub>2</sub>O<sub>3</sub> [36], CeO [37] etc. are the most widely used nanofiller in various types of nanocomposites. Some of these nano-oxides are also used as inert filler.

### **1.3.3 Metallic nanoparticles**

Metallic nanoparticles have fascinated over a century and are heavily utilized in biomedical sciences and engineering. This is primarily due to the fact that these materials can be synthesized and modified with appropriate functional groups that would allow them to bind with drugs, antibodies, ligands etc. Most common metallic nanoparticles are silver [38], palladium [39] and gold [40] fillers. Silver nanoparticles have gained tremendous acceptance due to their unique optical, electrical and thermal properties and range from solar cells to chemical sensors. Silver nanoparticles are widely used in antimicrobial coatings, textiles, plastics, wound dressing and biomedical devices. Gold nanoparticles are widely used due to its easy modification with the agents like therapeutic agents, drugs, ligands, etc. It is also used in imaging applications such as cancer imaging by selectively transporting gold nanoparticles in to the cancer cells. Moreover, the use of gold nanoparticle and nanorods are used in certain therapies such as photo thermal therapy. Some metallic nanoparticles exhibit electrical, magnetic and catalytic activity. These properties are used in nanocomposite with a wide range.

### **1.3.4 Nanocellulosic materials**

Nanocellulosic materials mean cellulose nanocrystals, cellulose nanofiber, carboxylated cellulose nanocrystals etc. are widely used as nanofiller in polymeric nanocomposite [41, 42].

Cellulose nanofillers are interesting materials for the preparation of low cost, lightweight, and high-strength nanocomposites [43]. As cellulose is biodegradable, nontoxic, highly dispersive and renewable in nature hence its usage is increasing day by day. Cellulosic nanofillers enhance better performance in thermal, mechanical, optical and dispersive properties of the nanocomposite.

## 1.4 Cellulose

Cellulose is the most abundant natural biopolymer available on the earth and it is a structural constituent of the cell wall of various plants. It is important not only for plant growth and development but also for industrial use. Apart from plants, cellulose is also present in a wide variety of living species, such as algae, fungi, bacteria, and even in some sea animals such as tunicates [44]. Cellulose is a fibrous, tough, and water-insoluble polymer and it plays an important role in maintaining the structure of plant cell walls. The chemical structure of cellulose is shown in figure 1.1.

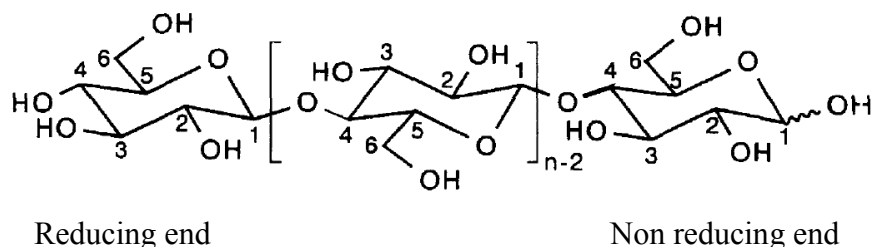


Figure 1.1 Typical structure of cellulose

It is basically a semicrystalline cellulose microfibril. It contains three different parts—a reducing end group with a free hemiacetal at the C<sub>1</sub> position, a non-reducing end group with a free hydroxyl group at the C<sub>4</sub> position, and internal anhydroglucopyranose rings joined at the C<sub>1</sub> and the C<sub>4</sub> positions through β 1-4 glycosidic bonds. The internal anhydroglucopyranose units are predominant due to the long chain lengths and contain three hydroxyl groups. The hydroxyl group at the C<sub>6</sub> position is a primary alcohol, while the hydroxyl groups at the C<sub>2</sub> and C<sub>3</sub> positions are secondary alcohols and these are corkscrewed at 180° with respect to its neighbors [45]. Due to the linear and quite regular structure of cellulose and having many hydroxyl groups, cellulose polymers can form ordered crystalline structures. These crystalline regions give important mechanical properties to the cellulose fibers. The hydroxyl groups in

the cellulose polymer can form hydrogen bonds between different cellulose polymers (intermolecular hydrogen bonds) or within the polymer itself (intramolecular hydrogen bonds). The intramolecular hydrogen bonds give stiffness to the polymer chain, while the intermolecular bonds allow the linear polymers to form sheet structures. With the van der Waal force, hydrogen bond helps to aggregate polymer chain together side-by-side and promotes parallel stacking of cellulose microfibrils into crystalline cellulose [46, 47]. The high crystallinity and the many hydrogen bonds in the cellulose fibers make cellulose insoluble in water and in most conventional organic solvents.

#### **1.4.1 Cellulose nanocrystal (CNC)**

Naturally occurring bulk cellulose consists of highly ordered, crystalline regions along with some disordered (amorphous) regions in varying proportions, depending on its source [48]. By removing amorphous regions applying mechanical, chemical or enzyme treatments we get highly ordered crystalline regions. These crystalline regions are referred to as whiskers, nanoparticles, nanofibers, microcrystallites, and so on, but the most widely accepted nomenclature is cellulose nanocrystals (CNCs). Generally CNCs are extracted by acid hydrolysis of cellulose [49]. Acid hydrolysis performed by using different acids like sulfuric acid, hydrochloric acid, phosphoric acid, hydrobromic acid, nitric acid, acetic acid and some mixture of acids [50, 51]. Among these acids sulfuric acid gives the best crystallinity index and hence it is used in a large scale. During sulphuric acid treatment, the hydronium ions migrate to the amorphous regions since they have lower density compared to the crystalline regions. The hydronium ions cleave the glycosidic linkages hydrolytically and thereby releasing the individual crystallites. Sulfuric acid treatments produce negatively surface charge which is very important for the dispersiveness of CNCs. On the other hand, hydrochloric acid or hydrobromic acid treatments don't produce surface charge and resulting CNCs aggregates and dispersion decreases. CNCs are spherical or stiff rod-like particles consisting of cellulose chain segments in a nearly perfect crystalline structure. Compare to native cellulose, which has greater amorphous fractions, these nanocrystals exhibit high specific strength, modulus, high surface area, and unique crystalline properties.

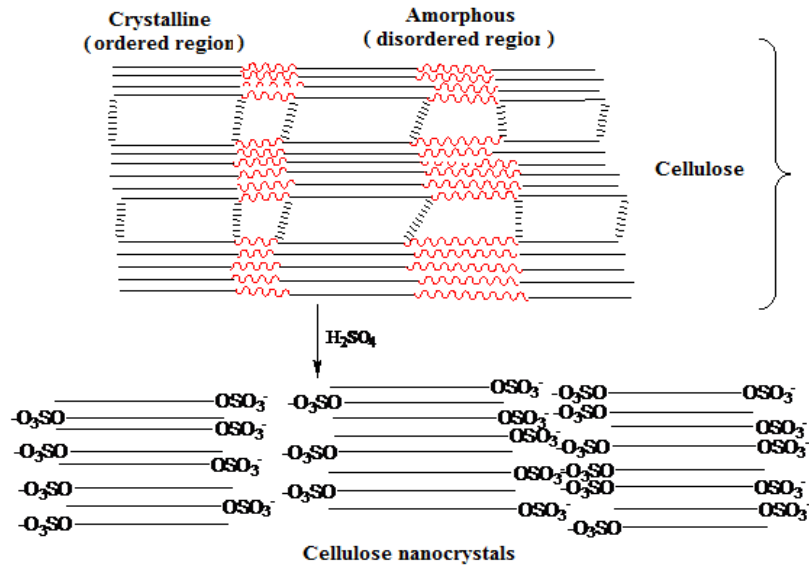


**Figure 1.2: Degradation of amorphous region of cellulose by sulfuric acid.**

CNCs have been extracted from different cellulose sources such as hardwood pulp [52], softwood pulp [53, 54], microcrystalline cellulose (MCC) [55], sisal [56], cotton [57], wheat straw [58], rice straw [59], bacterial cellulose [60], algae [55, 61], banana fibers [62], sugar beet [63], and tunicin [64]. Other biopolymers that have been reported to form nanocrystals during acid hydrolysis are chitin [65], potato pulp [66], yellow pea [67], and waxy maize [68]. Different types of cellulose sources give some different structures of the nanocrystals and the aspect ratio will differ for the different sources. CNCs have great potential application in bionanocomposites [69], aerogels for oil/water separation [70], protein immobilization [71], antimicrobial packagings [72], drug delivery [73] and metallic reaction templates [74]. CNC has multidimensional applications as it is non toxic, cheap, biocompatible and highly water dispersive. In case of environment remediation it acts as good adsorbent.

#### 1.4.2 Carboxylated cellulose nanocrystals (CCN)

As CNC has high crystallinity, dispersive property and great mechanical strength, it exhibits multidimensional application in different fields. But in case of wastewater management, the application of CNCs is much less explored because it aggregates due to the formation of tightly hydrogen bonded networks as the surface of CNC has numerous hydroxyl groups. The aggregation of CNC can be reduced by surface modification. Generally the surface of CNCs

is modified by esterification, etherification, oxidation, amidation, carbamation, nucleophilic substitution, silylation, polymer grafting, etc. by introducing negative or positive charge on the surface of CNC provides better dispersion in any solvent. By oxidation reaction surface hydroxyl group converted to carboxyl group which ultimate produce negative charge on the surface. Carboxyl group containing CNC is called CCN, which acts as efficient adsorbent for removal of dye and heavy metals. Recently, 2, 2, 6, 6-tetramethylpiperidine-1-oxyl radical (TEMPO) mediated oxidation [75-78], periodate-chlorite oxidation [79-83] and ammoniumpersulfate (APS) oxidation [84, 85] have been used to produce CCN. In case of periodate-chlorite treatment of CNC, periodate selectively oxidize C<sub>2</sub> and C<sub>3</sub> hydroxyl groups to two aldehyde groups and then to carboxyl groups. During periodate treatment it breaks down the pyranose ring of the glucose unit and may decrease molecular chain lengths or rigidity of the CNCs [81, 82, 86]. Periodate is toxic as well as expensive and as it is two step process, it requires more time. On the other hand TEMPO mediated oxidation selectively oxidize C<sub>6</sub> hydroxyl group to carboxyl group and it is one step process; it requires comparatively lesser time and the pyranose ring remains intact. As a result, rigidity of CCNs remains same with CNCs after carboxylation of CNCs.

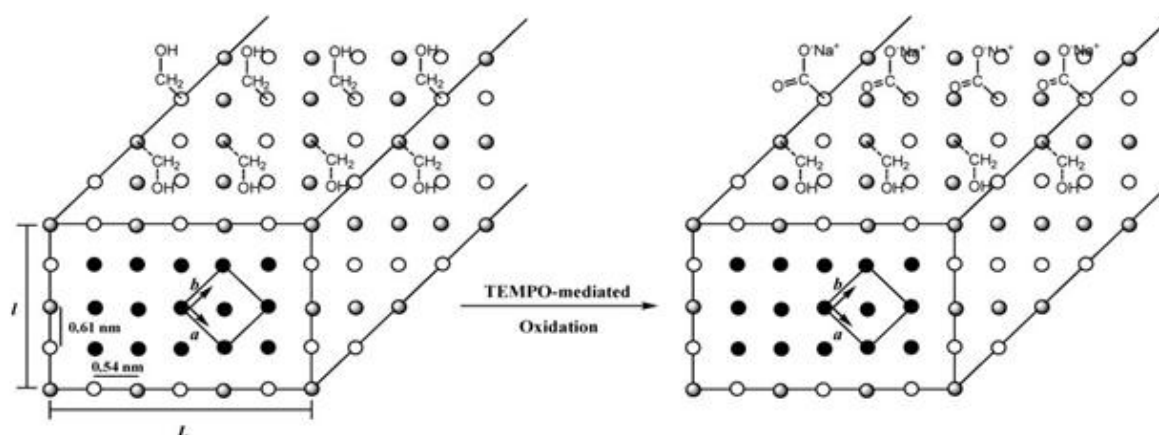


Figure 1.3 Cross sectional representation of cellulose nanocrystal indicating the occurrence of the surface TEMPO-mediated oxidation of available hydroxyl groups

Surface carboxylated CNCs with different sizes and degrees of oxidation were prepared by TEMPO-mediated oxidation of cellulose, and they showed higher adsorption capacity for cationic dyes (769 mg dye/g CNC) than that of unmodified CNCs [87, 88]. TEMPO-mediated oxidation involves a topologically confined reaction sequence, and as a

consequence of the 2-fold screw axis of the cellulose chain, only half of the accessible hydroxymethyl groups are available to react, whereas the other half are buried within the crystalline particle.

## 1.5 Crosslinker

Crosslinking is the process of chemically joining two or more molecules or polymer chains by a covalent bond. Generally, which agents perform this joining work is called crosslinker. Crosslinkers contain at least two reactive groups. Reactive groups that can be targeted for crosslinking include primary amines, sulfhydryls, carbonyls, vinyl group, carbohydrates, carboxylic acids etc. When polymer chains are linked together by cross-linker, they lose some of their ability to move as individual polymer chains. Hence chemical crosslinking are mechanically and thermally stable. Crosslinking may be initiated by heat, pressure, change in pH, or radiation. Crosslinkers are chosen depending on chemical specificity, same or different reactive groups, spontaneously reactive or photoreactive groups etc. Crosslinkers are commonly used to modify nucleic acids, drugs and solid surfaces.

### 1.5.1 Linear crosslinker

In this group of crosslinker the reactive groups are usually remain at the end of chain. It is also called 1D crosslinker. 1D crosslinker contains at least two active sites which are able to react with substrate or polymer matrix. Due to lower active sites comparatively less amount of polymer chains are linked up. Commonly used linear crosslinkers are methylene-bis-acrylamide(MBA), bis(triethoxysilylpropyl)tertarsulfide, imidoester etc.

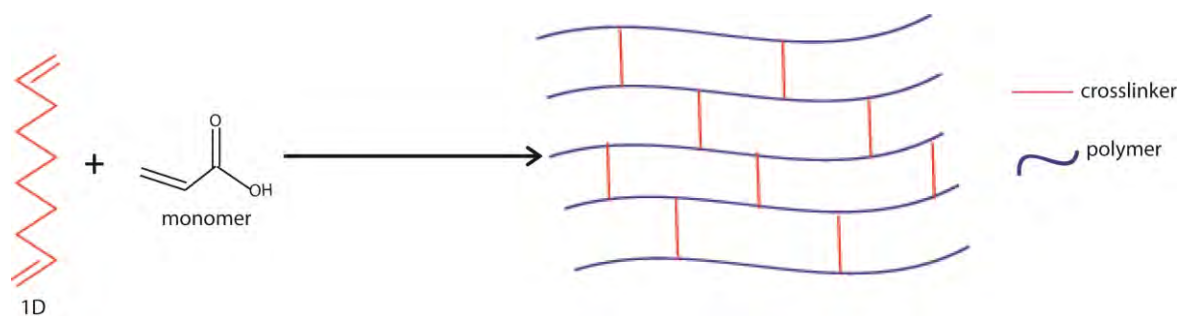


Figure 1.4 Synthesis of nanocomposite using 1D crosslinker



### 1.5.2 Planar (2D) crosslinker

Planar crosslinkers are normally called 2D crosslinker. Its reactive groups are on the upper and lower side of the surface. In case of linear crosslinker there are only two linking sites. But in case of 2D crosslinker many more active sites are available on the surface. These active sites interact with the coming group of polymer or other matrices and form an excellent composite material. 2D crosslinkers are able to link comparatively higher number of polymer chains. As a result different physical and chemical properties are improved by using 2D crosslinker. Well known 2D crosslinkers included nanoclay, graphene oxide (GO) nanoparticles, functionalized GO etc. are widely used to form nanocomposite. These nanocomposites are used in wastewater treatment, electronic devices and many more sectors.

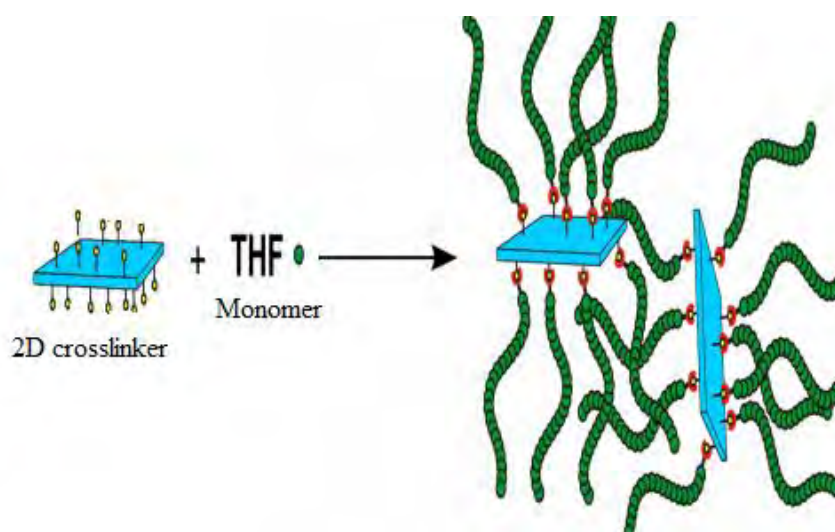


Figure 1.5 Synthesis of nanocomposite using 2D crosslinker  
Tasdelen et al, *Macromolecules*, 2008, 41, 6035-6040.

### 1.5.3 Three dimensional crosslinker

This class of crosslinkers added new dimension in the crosslinked composite materials. The shape of the 3D crosslinker may be spherical. Its surface area is comparatively higher than that of the linear or planar crosslinker. In case of 2D crosslinker only two sides contain active sites for the interaction with substrate but in case of 3D crosslinker, reactive sites are laying all sides of 3D crosslinker. Hence it contains a wide number of reactive sites in a small surface area. Due to this its reactivity increases dramatically. Since reactive sites are scattered, 3D crosslinkers are able to link with much more polymer chains. As a result the



produced nanocomposite become robust and improved chemical and mechanical properties of the nanocomposites.

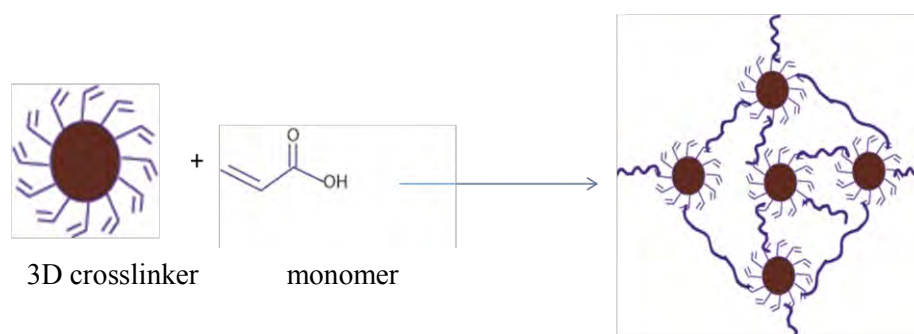


Figure 1.6 Synthesis of nanocomposite using 3D crosslinker

### 1.6 Magnetically responsive polymer nanocomposite

During the last decade, the development of magnetic polymer nanocomposite materials has been the source of discovery of spectacular new phenomena, with potential applications in the multidimensional fields. Among the broad spectrum of nanoscale materials being investigated for various environmental and biomedical applications, magnetic nanoparticles (MNPs) have gained significant attention due to their intrinsic magnetic properties, which makes them successful as magnetically recoverable catalysts, drug delivery agents, anticancer materials, magnetic resonance imaging devices, etc. Magnetic nanoparticles and nanocomposites have aroused significant scientific and technological interest because of their potential applications in the fields of biomedicine, information technology, magnetic resonance imaging, catalysis, telecommunication, and environmental remediation [3–6]. Magnetic polymer nanocomposites generally comprise of magnetic nanoparticles embedded in polymer matrix. However, magnetic nanoparticles dispersed in composites usually have a strong tendency to form agglomerates for reduction of energy associated with high surface area-to-volume ratio of the nanosized particles. To avoid aggregation of magnetic nanoparticles, protection strategies have been developed to chemically stabilize the magnetic nanoparticle. The properties of magnetic particles remain same after stabilization. So its application in polymer nanocomposites is increasing day by day.

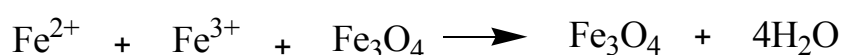
### 1.7 Magnetic nanoparticles

In nature iron oxides exist in many forms like magnetite ( $\text{Fe}_3\text{O}_4$ ), hematite ( $\alpha\text{-Fe}_2\text{O}_3$ ) and maghemite ( $\gamma\text{-Fe}_2\text{O}_3$ ). Among these oxides  $\text{Fe}_3\text{O}_4$  particles are more demandable due to

surface efficiency. The surface area of iron-oxide-based magnetic materials decreased their response to external magnetic field making it difficult to recover the adsorbents after treatment has been completed. On the other hand, the adsorption capacities of adsorbents rely largely on the available surface areas, and the increase of the surface area is normally obtained by the decrease of the particle size of adsorbents. As a result, there is a need to synthesize such adsorbents with proper particles size for the removal of dye or heavy metals from industrial wastewater. Up to date, there are many methods to synthesize ironoxide nanoparticle. The most common methods include co-precipitation, hydrothermal synthesis, thermal decomposition, sol-gel method and colloidal chemistry method. Among these methods, coprecipitation has proven to be the most promising method for the production of iron oxide nanoparticles as the procedure is relatively simple and the particles can be obtained with controlled particle size.

### 1.7.1 Co-precipitation method

The most conventional method for obtaining  $\text{Fe}_3\text{O}_4$  is co-precipitation. This method consists of mixing ferrous and ferric ions in a 2:1 molar ratio in highly basic solutions at room temperature or at elevated temperature. The chemical reaction of  $\text{Fe}_3\text{O}_4$  formation may be written as



The size and shape of the iron oxide nanoparticles depend on the type of salts used (such as chlorides, sulfates, nitrates, perchlorates, etc.), the ferric and ferrous ions ratio, the reaction temperature, the pH value, and the other reaction parameters (e.g. stirring rate, dropping speed of basic solution).  $\text{Fe}_3\text{O}_4$  nanoparticles are not very stable under normal conditions and are easily oxidized.



In order to avoid the possible oxidation in the air, the synthesis of  $\text{Fe}_3\text{O}_4$  NPs must be done in an inert atmosphere.

### 1.7.2 Surface modification of iron oxide nanoparticle

Bare iron oxide nanoparticles tend to aggregate because of strong magnetic attractions among particles, the van der Waal force and high surface energy. On the other hand when the magnetic nanoparticles are in contact of air, these particles are further oxidized to form alpha or gamma  $\text{Fe}_2\text{O}_3$ . To avoid this problem surface of iron oxide nanoparticles are coated to improve their stability and biocompatibility and to achieve hydrophilicity and conjugating capability. Several coating materials including organic polymers (e.g. dextran, chitosan, polyethylene glycol), organic surfactants (e.g. sodium oleate and dodecylamine), inorganic metals (e.g. gold), inorganic oxides (e.g. silica and carbon) etc. are used to modify the surface of the magnetic nanoparticles.

### 1.8 Research goal

In this research, the main objective is to fabricate a novel magnetic nanocomposite using 3D crosslinker and cellulosic material via in situ polymerization. When nanocomposite used as adsorbent, there is a challenging issue to separate them. The separation of nonmagnetic nanocomposite after using as adsorbent is very complex, lengthy and tedious. Magnetic nanocomposite is an excellent nanomaterials for wastewater management due to its easy separation process and its demand increasing day by day. From the literature review it was seen that magnetic nanocomposites contain magnetic nanoparticles embedded on the polymer matrix and they were loosely bound to the polymer chain with van der Waal force. When the magnetic field is applied then only the magnetic particles attracted by the magnet and separate leaving the polymer chain as the polymer chains are not directly linked with magnetic particles. So the nanocomposites are not possible to recycle or reuse. Hence this type of nanocomposite can use only one time. As a result its usage is expensive. Nanocomposites can be recycled and reused if the magnetic particles are directly linked with the polymer chains. Herein, we plan to modify magnetic particles by acrylic group and this acrylic group directly linked with polymer chain by strong covalent bond. This acrylic modified magnetic particles act as 3D crosslinker which has more reactive sites than conventional linear or planar crosslinker and resulting make the composite much more sticky and adhesive. So another approach is to decrease this adhesive property and increase dispersive property. For this purpose, carboxylated cellulose nanocrystals, which are highly dispersive in most of the solvent, are incorporated in the composite. Finally, more reactive

sites containing 3D crosslinker, highly dispersive carboxylated cellulose nanocrystals and acrylic acid monomer are used to synthesize a new magnetic nanocomposite via in situ polymerization using potassium per sulfate as initiator. Thus produced nanocomposite would characterize by x-ray photoelectron spectroscopy (XPS), x-ray diffraction (XRD), scanning electron microscopy (SEM), energy dispersive x-ray (EDX), thermogravimetric analysis (TGA), fourier transform infrared (FTIR) analyses. The possible outcome of the current research is to develop a 3D crosslinker, a new facile method for the fabrication of a novel magnetic nanocomposite containing a manifold carboxyl group. This nanocomposite may be used for the removal of cationic dye and heavy metals from the wastewater.

## References

1. Camargo, P. H. C.; Satyanarayana, K. G.; Wypych, F.; “Nanocomposites: Synthesis, Structure, Properties and New Application Opportunities”, *Mater. Res.*, vol. 12(1), pp. 1-39, 2009.
2. Zhu, J.; Wei, S.; Chen, M.; Gu, H. ; Rapole, S. B.; Pallavkar, S.; C. Ho, T.; Hopper, J.; Guo, Z.; “Magnetic nanocomposites for environmental remediation”, *Adv. Powder Tech.*, vol. 24, pp. 459–467, 2013.
3. Jafarbeglou, M.; Abdouss, M.; . Shoushtari, A. M.; Jafarbeglou, M.; “Clay nanocomposites as engineered drug delivery systems”, *RSC Adv.*, vol. 6, pp. 50002-50016, 2016.
4. Iliescu, R. I.; Andronescu, E.; Ghitulica, C. D.; Voicu, G.; Ficai, A.; Hoteteu, M.; “Montmorillonite–alginate nanocomposite as a drug delivery system – incorporation and in vitro release of irinotecan”, *Int. J. Pharma.*, vol. 463, pp. 184–192, 2014.
5. Jones, W. E.; Chiguma, J.; Johnson, E.; Pachamuthu, A.; Santos, D.; “Electrically and Thermally Conducting Nanocomposites for Electronic Applications”, *Materials*, vol. 3, pp. 1478-1496, 2010.
6. Zhang, S.; Sun, D.; Fu, Y.; Du, H.; “Recent advances of superhard nanocomposite coatings: a review”, *Surf. Coat. Technol.*, vol. 167, pp. 113–119, 2003.
7. Hauert, R.; Patscheider, J.; “From alloying to nanocomposites – improved performance of hard coatings”, *Adv. Eng. Mater.*, vol. 2, pp. 247 – 59, 2000.

8. Zang, Z.; Chen, D. L.; “Consideration of Orowan strengthening effect in particulate-reinforced metal matrix nanocomposites: A model for predicting their yield strength”, *Scripta Materialia*, vol. 54, pp. 1321-1326, 2006.
9. Rohatgi, P. K.; Schultz B.; “Lightweight Metal Matrix Nanocomposites - Stretching the Boundaries of Metals”, *Mater. Mat.*, vol. 2.4, pp. 16, 2007.
10. Hossein-Zadeh, M.; Razavi, M.; Mirzaee, O.; Ghaderi, R.; “Characterization of properties of Al–Al<sub>2</sub>O<sub>3</sub> nano-composite synthesized via milling and subsequent casting”, *J. King Saud University – Eng. Sci.*, vol. 25, pp. 75–80, 2013.
11. Chu, H.; Zhang, J.; An, M.; “Influences of SiC Concentration on Sn/SiC Nanocomposite Electrodeposition”, *Int. J. Electrochem. Sci.*, vol. 8, pp. 1871 – 1884, 2013.
12. Paramsothy, M.; Chan, J.; Kwok, R.; Gupta, M.; “TiC nanoparticle addition to enhance the mechanical response of hybrid magnesium alloy”, *J. Nanotech.*, vol. 2012, Article ID 401574, 9 pages, 2012.
13. Zhou, C.; Wu, Q.; “A novel polyacrylamide nanocomposite hydrogel reinforced with natural chitosan nanofibers”, *Colloids and Surfaces B: Biointerfaces*, vol. 84, pp. 155–162, 2011.
14. Feldman, D.; “Poly(vinyl chloride) Nanocomposites”, *J. Macromol. Sci. A, Pure and Appl. Chem.*, vol. 51, pp. 659–667, 2014.
15. Ciprari, D.; Jacob, K.; Tannenbaum, R.; “Characterization of polymer nanocomposite interphase and its impact on mechanical properties”, *Macromol.*, vol. 39, pp. 6565-6573, 2006.
16. He, J.; Shen, Y.; Yang, J.; Evans, D. G.; Duan, X.; “Nanocomposite structure based on silylated mcm-48 and poly(vinyl acetate)”, *Chem. Mater.*, vol. 15, pp. 3894-3902, 2003.
17. Lai, G. S.; Lau, W. J.; Gray, S. R.; Matsuura, T.; Gohari, R. Ja.; Subramanian, M. N.; Lai, S. O.; Ong, C. S.; Ismail, A. F.; Emazadah, D.; Ghanbari, M.; “A practical approach to synthesize polyamide thin film nanocomposite (TFN) membranes with improved separation properties for water/wastewater treatment”, *J. Mater. Chem., A*, vol. 4, pp. 4134-4144, 2016.
18. Shahabuddin, S.; Sarih, N. M.; Kamboh, M. A.; Nodeh, H. R.; Mohamad, S.; “Synthesis of Polyaniline-Coated Graphene Oxide@SrTiO<sub>3</sub> Nanocube Nanocomposites for Enhanced Removal of Carcinogenic Dyes from Aqueous Solution”, *Polymer.*, vol. 8(9), pp. 305, 2016.

19. Andu, Y.; Jeong, J.M.; Nishida, H.; Endo, T.; “Simple procedure for polystyrene-based nanocomposite preparation by vapor-phase-assisted surface polymerization”, *Macromol.*, vol. 42 (20), pp. 7930–7935, 2009.
20. Liu, P.S.; Li, L.; Zhou, N.L.; Zhang, J.; Wei, S.H.; Shen, J.; “Synthesis and properties of a poly(acrylic acid)/ montmorillonite superabsorbent nanocomposite”, *J. Appl. Polym. Sci.*, vol. 102, pp. 5725–5730, 2006.
21. Bragov, A. M.; Igumnov, L. A.; Konstantinov, A. Yu.; Lomunov, A. K.; Antonov, F. K.; Mossakovskii, P. A.; “Impact compressibility of a poly(ethylene glycol)-based nanocomposite fluid”, *Tech. Physic. Lett.*, vol. 40, pp. 923–925, 2014.
22. Lee, C.; Jug, L.; Meng, E.; “High strain biocompatible polydimethylsiloxane-based conductive graphene and multiwalled carbon nanotube nanocomposite strain sensors”, *Appl. Physic. Lett.*, vol. 102, pp. 183511, 2013.
23. Saboktakin, A.; Saboktakin, M. R.; “Improvement of reinforced concrete properties based on modified starch/polybutadiene nanocomposites”, *Macromol. Biol. J. Int.*, vol. 70, pp. 381–384, 2014.
24. Henriette, M.C.; de Azeredo,.; “Nanocomposites for food packaging applications”, *Food Res. Int.*, vol. 42, pp. 1240–1253, 2009.
25. Hari, J.; Pukanzsky, B.; Nanocomposites: Preparation, structure, properties. In *Applied Plastics Engine Handbook: Processing Materials*; Kutz, M., Ed.; Elsevier Inc.: Waltham, MA, USA, pp. 109–142, 2011
26. Marquis, D.M.; Guillaume, É.; Joly, C. C.; Properties of nanofillers in polymer. In *Nanocomposites and Polymers with Analytical Methods*; Cuppoletti, J., Ed.; Intech Publishing: Rijeka, Croatia, 2011, 261–284.
27. Kango, S.; Kalia S.; Celli, A.; Njuguma, J.; Habibi, Y.; Kumar, R.; “Surface modification of inorganic nanoparticles for development of organic–inorganic nanocomposites”, *Prog. Polym. Sci.* vol. 38, pp. 1232–1261, 2013.
28. Ciprari, D.; Jacob, K.; Tannenbaum, R.; “Characterization of polymer nanocomposite interphase and its impact on mechanical properties”, *Macromol.*, vol. 39, pp. 6565–6573, 2006.
29. Liu, T.; Lim, K. P.; Tjiu, W.C.; Pramoda, K. P.; Chen, Z. K.; “Preparation and characterization of nylon 11/organoclay nanocomposites”, *Polymer*, vol. 44, pp. 3529–3535, 2003.

30. Lateef, A.; Nazir, R.; Jamil, N.; Alam, S.; Shah, R.; Khan, M. N.; Saleem, M.; “Synthesis and characterization of zeolite based nano-composite: An environment friendly slow release fertilizer”, *Micropor. Mesopor. Mater.*, vol. 232, pp. 174–183, 2016.
31. Zou, H.; Wu, S.; Shen, J.; “Polymer/Silica Nanocomposites: Preparation, Characterization, Properties, and Applications”, *Chem. Rev.*, vol. 108, pp. 3893–3957, 2008.
32. Vu, Q. T.; Pavlik, M.; Hebestreit, N.; Rammelt, U.; Plieth, W.; Pflüge, J.; “Nanocomposites based on titanium dioxide and polythiophene: Structure and properties”, *Reac. Func. Polym.*, vol. 65, pp. 69–77, 2005.
33. Ma, J.; Zhu, W.; Tian, Y.; Wang, Z.; “Preparation of Zinc Oxide-Starch Nanocomposite and Its Application on Coating”, *Nanoscale Res. Lett.*, vol. 11, pp. 200, 2016.
34. Sato, M.; Kawata, A.; Morito, S.; Sato, Y.; Yamaguchi, I.; “Preparation and properties of polymer/zinc oxide nanocomposites using functionalized zinc oxide quantum dots”, *Eur. Polym. J.*, vol. 44, pp. 3430–3438, 2008.
35. Chen, C.H.; Jian, J.Y.; Yen, F. S.; “Preparation and characterization of epoxy/ $\gamma$ -aluminum oxide nanocomposites”, *Composites Part A: Appl. Sci. Manufac.*, vol. 40, pp. 463–468, 2009.
36. Liang, Y.; Xia, X.; Luo, Y.; Jia, Z.; “Synthesis and performances of  $\text{Fe}_2\text{O}_3$ /PA-6 nanocomposite fiber”, *Mater. Lett.*; vol. 61, pp. 3269–3272, 2007.
37. Kumar, E.; Selvarajan, P.; Muthuraj, D.; “Preparation and characterization of polyaniline/cerium dioxide (CeO) nanocomposite via in situ polymerization”, *J. Mater. Sci.*, vol. 47, pp. 7148, 2012.
38. Zapata, P. A.; Tamayo, L.; Páez, M.; Cerda, E.; Azócar, I.; Rabagliati, F. M.; “Nanocomposites based on polyethylene and nanosilver particles produced by metallocenic “in situ” polymerization: synthesis, characterization, and antimicrobial behavior”, *Eur. Polym. J.*, vol. 47, pp. 1541–1549, 2011.
39. Melinger, J. S.; Kleiman, V. D.; McMorro, D.; “Ultrafast Dynamics of Gold-Based Nanocomposite Materials”, *J. Phys. Chem. A*, vol. 107, pp. 3424–3431, 2003.
40. Onbattuvelli, V.; Ostroverkhova, O.; Mulla, I.S.; Pillai, V. K.; Atre S.; “The effect of synthesis procedure on the structure and properties of palladium/polycarbonate nanocomposites”, *Polymer*, vol. 49, pp. 3413–3418, 2008.

41. Dong, H.; Strawhecker, K. E.; Snyder, J. F.; Orlicki, J. A.; Reiner, R.S.; Rudie, A.W.; “Cellulose nanocrystals as a reinforcing material for electrospun poly(methyl methacrylate) fibers: formation, properties and nanomechanical characterization”, *Carbohydr. Polym.*, vol. 87, pp. 2488–2495, 2012.
42. Ten, E.; Turtle, J.; Bahr, D.; Jiang, L.; Wolcott, M.; “Thermal and mechanical properties of poly(3-hydroxybutyrate-co-3-hydroxyvalerate)/cellulose nanowhiskers composites”, *Polymer*, vol. 51, pp. 2652–2660, 2010.
43. Podsiadlo, P.; Choi, S. Y.; Shim, B.; Lee, J.; Cuddihy, M.; Kotov, N. A.; “Molecularly engineered nanocomposites: Layer-by-layer assembly of cellulose nanocrystals”, *Biomacromol.*, vol. 6, pp. 2914-2918, 2005.
44. Klemm, D.; Heublein, B.; Fink, H. P.; Bohn, A.; “Cellulose: fascinating biopolymer and sustainable raw material”, *Chem. Int. Ed. Engl.* vol. 44(22), pp. 3358-93, 2005.
45. Habibi, Y.; Lucia, L. A.; Rojas, O. J.; “Cellulose nanocrystals: chemistry, self-assembly, and applications”, *Chem. Rev.*, vol. 110 (6), pp. 3479-500, 2010.
46. Brett, C. T.; “Cellulose microfibrils in plants: biosynthesis, deposition, and integration into the cell wall”, *Int. Rev Cytol.*, vol. 199, pp.161-199, 2000.
47. Somerville, C.; “Cellulose synthesis in higher plants”, *Annu. Rev Cell Dev Biol.* vol. 22, pp. 53-78, 2006.
48. Newman, R. H.; Hemmingson, J. A.; “Carbon-13 NMR distinction between categories of molecular order and disorder in cellulose”, *Cellulose*, vol. 2, pp. 95–110, 1994.
49. Domingues, R. M.; Gomes, M. E.; Reis, R. L, “The potential of cellulose nanocrystals in tissue engineering strategies”, *Biomacromol.*, vol. 15, pp. 2327–2346, 2014.
50. Houyong, Yu.; Zongyi, Qin.; Liang, B.; Liu, N.; Zhou, Z.; Chen, L.; “Facile extraction of thermally stable cellulose nanocrystals with a high yield of 93% through hydrochloric acid hydrolysis under hydrothermal conditions”, *J. Mater. Chem., A*, vol. 1, pp. 3938-3944, 2013.
51. Espiona, C.; Kuhnt, T.; Foster, E. J.; Weder, C.; “Isolation of thermally stable cellulose nanocrystals by phosphoric acid hydrolysis”, *Biomacromol.*, vol. 14(4), pp. 1223-30, 2013.
52. Nishiyama, Y.; Kim, U. J.; Kim, D. Y.; Katsumata, K. S.; May, R. P.; Langan, P.; “Periodic disorder along ramie cellulose microfibrils”, *Biomacromol.*, vol.4, pp. 1013–1017, 2003.



53. Hafraoui, S. E.; Nishiyama, Y.; Putaux, J. L.; Heux, L.; Dubreuil, F.; Rochas, C.; “The shape and size distribution of crystalline nanoparticles prepared by acid hydrolysis of native cellulose”, *Biomacromol.* vol. 9, pp. 57–65, 2008.
54. Candanedo S. B.; Roman, M.; Gray, D. G.; “Effect of reaction conditions on the properties and behavior of wood cellulose nanocrystal suspensions”, *Biomacromol.*, vol. 6, pp. 1048–1054, 2005.
55. De Rodriguez, N.; Thielemans, W.; Dufresne, A.; “Sisal cellulose whiskers reinforced polyvinyl acetate nanocomposites”, *Cellulose*, vol. 13, pp. 261–270, 2006.
56. Kimura, F.; Kimura, T.; Tamura, M.; Hirai, A.; Ikuno, M.; Horii, F.; “Magnetic alignment of the chiral nematic phase of a cellulose microfibril suspension”, *Langmuir*, vol. 21, pp. 2034–2037, 2005.
57. George, J.; Bawa, A.S.; Siddaramiah; “Synthesis and characterization of bacterial cellulose nanocrystals and their PVA nanocomposites”, *Adv. Mater. Res.*, vol. 123, pp. 383–386, 2010.
58. Moon, R. J.; Martini, A.; Nairn, J.; Simonsen, J.; Youngblood, J.; “Cellulose nanomaterials review: structure, properties and nanocomposites”, *Chem. Soc. Rev.*, vol. 40, pp. 3941–3994, 2011.
59. Iwamoto, S.; Kai, W.; Isogai, A.; Iwata, T.; “Elastic modulus of single cellulose microfibrils from tunicate measured by atomic force microscopy”, *Biomacromol.*, vol. 10, pp. 2571–2576, 2009.
60. Lahiji, R. R.; Xu, X.; Reifenberger, R.; Raman, A.; Rudie, A.; Moon, R. J.; “Atomic force microscopy characterization of cellulose nanocrystals”, *Langmuir*, vol. 26, pp. 4480–4488, 2010.
61. Sturcova, A.; Davies, G. R.; Eichhorn, S. J.; “Elastic modulus and stress-transfer properties of tunicate cellulose whiskers”, *Biomacromol.*, vol. 6, pp. 1055–1061, 2005.
62. Brinchi, L.; Cotana, F.; Fortunati, E.; Kenny, J. M.; “Production of nanocrystalline cellulose from lignocellulosic biomass: technology and applications”, *Carbohydr Polym.*, vol. 94, pp. 154–169, 2013.
63. Azizi Samir, M. A. S.; Alloin, F.; Paillet, M.; Dufresne, A.; “Tangling effect in fibrillated cellulose reinforced nanocomposites”, *Macromol.*, vol. 37, pp. 4313–4316, 2004.

64. Bonini, C.; Heux, L.; Cavaille, J.Y.; Lindner, P.; Dewhurst, C.; Terech, P.; “Rodlike cellulose whiskers coated with surfactant: A small-angle neutron scattering characterization”, *Langmuir*, vol. 18, pp. 3311-3314, 2002.
65. Lam, E.; Male, K. B.; Chong, J. H.; Leung, A. C.; Luong, J. H.; “Applications of functionalized and nanoparticle-modified nanocrystalline cellulose”, *Trends Biotech.*, vol. 30, pp. 283–290, 2012.
66. Jackson, J. K.; Letchford, K.; Wasserman, B. Z.; Ye, L.; Hamad, W. Y.; Burt, H. M.; “The use of nanocrystalline cellulose for the binding and controlled release of drugs”, *Int. J. Nanomed.*, vol. 6, pp. 321, 2011.
67. Nogi, M.; Iwamoto, S.; Nakagaito, A. N.; Yano, H.; “Optically transparent nanofiber paper”, *Adv. Mater.*, vol. 21, pp. 1595–1598, 2009.
68. Belbekhouche, S.; Bras, J.; Siqueira, G.; Chappey, C.; Lebrun, L.; “Water sorption behavior and gas barrier properties of cellulose whiskers and microfibrils films”, *Carbohydr. Polym.*, vol. 83, pp. 1740–1748, 2011.
69. Yu, H.; Sun, B.; Zhang, D.; Chen, G.; Yang, X.; Yao, J.; “Reinforcement of biodegradable poly(3-hydroxybutyrate-co-3-hydroxyvalerate) with cellulose nanocrystal/silver nanohybrids as bifunctional nanofillers”, *J. Mater. Chem. B*, vol. 2 (48), pp. 8479-8489, 2014.
70. Dash, R.; Li, Y.; Ragauskas, A. J.; “Cellulose nanowhisker foams by freeze casting”, *Carbohydr. Polym.*, vol. 88 (2), pp. 789-792, 2012.
71. Yu, H.; Chen, G.; Wang, Y.; Yao, J.; “A facile one-pot route for preparing cellulose nanocrystal/zinc oxide nanohybrids with high antibacterial and photocatalytic activity”, *Cellulose*, vol. 22 (1), pp. 261-273, 2015.
72. Fortunati, E.; Armentano, I.; Zhou, Q.; Iannoni, A.; Saino, E.; Visai, L.; Berglund, L. A.; Kenny, J. M.; “Multifunctional bionanocomposite films of poly(lactic acid), cellulose nanocrystals and silver nanoparticles”, *Carbohydr. Polym.*, vol. 87 (2), pp. 1596-1605, 2012.
73. Wang, H.; He, J.; Zhang, M.; Tam, K. C.; Ni, P.; “A new pathway towards polymer modified cellulose nanocrystals via a “grafting onto” process for drug delivery”, *Polym. Chem.*, vol. 6, pp. 4206-4209, 2015.
74. Padalkar, S.; Capadona, J. R.; Rowan, S. J.; Weder, C.; Moon, R. J.; Stanciu, L. A.; “Self-assembly and alignment of semiconductor nanoparticles on cellulose nanocrystals”, *J. Mater. Sci.*, vol. 46 (17), pp. 5672-5679, 2011.

75. Wang, Y.; Chen, L.; “Cellulose nanowhiskers and fiber alignment greatly improve mechanical properties of electrospun prolamin protein fibers”, *ACS Appl. Mater. Inter.*, vol. 6 (3), pp. 1709-1718, 2014.
76. Lin, N., Bruzzese, C.; Dufresne, A.; “TEMPO-oxidized nanocellulose participating as crosslinking aid for alginate-based sponges”, *ACS Appl. Mater. Inter.*, vol. 4 (9), 4948-4959, 2012.
77. Peyre, J.; Pääkkönen, T.; Reza, M.; Kontturi, E.; “Simultaneous preparation of cellulose nanocrystals and micron-sized porous colloidal particles of cellulose by TEMPO-mediated oxidation”, *Green Chem.*, vol. 17 (2), pp. 808-811, 2015.
78. Rafieian, F.; Shahedi, M.; Keramat, J.; Simonsen, J.; “Mechanical, thermal and barrier properties of nano-biocomposite based on gluten and carboxylated cellulose nanocrystals”, *Int. Crop. Prod.*, vol. 53, pp. 282-288, 2014.
79. Drogat, N.; Granet, R.; Sol, V.; Memmi, A.; Saad, N.; Koerkamp, C. K.; Bressollier, P.; Krausz, P.; “Antimicrobial silver nanoparticles generated on cellulose nanocrystals”, *J. Nanopart. Res.*, vol. 13(4), pp. 1557-1562, 2011.
80. Visanko, M.; Liimatainen, H.; Sirviö, J. A.; Heiskanen, J. P.; Niinimäki, J.; Hormi, O.; “Amphiphilic cellulose nanocrystals from acid-free oxidative treatment: physicochemical characteristics and use as an oil-water stabilizer”, *Biomacromol.*, vol. 15 (7), pp. 2769-2775, 2014.
81. Sun, B.; Hou, Q.; Liu, Z.; Ni, Y.; “Sodium periodate oxidation of cellulose nanocrystal and its application as a paper wet strength additive”, *Cellulose*, vol. 22 (2), pp. 1135-1146, 2015.
82. Liimatainen, H.; Visanko, M.; Sirviö, J.; Hormi, O.; Niinimäki, J.; “Sulfonated cellulose nanofibrils obtained from wood pulp through regioselective oxidative bisulfate pre-treatment”, *Cellulose*, vol. 20 (2), pp. 741-749, 2013.
83. Liimatainen, H.; Visanko, M.; Sirviö, J.; Hormi, O.; Niinimäki, J.; “Enhancement of the nanofibrillation of wood cellulose through sequential periodate-chlorite oxidation”, *Biomacromol.*, vol. 13 (5), pp. 1592-1597, 2012.
84. Cheng, M.; Qin, Z.; Liu, Y.; Qin, Y.; Li, T.; Chen, L.; Zhu, M.; “Efficient extraction of carboxylated spherical cellulose nanocrystals with narrow distribution through

- hydrolysis of lyocell fibers by using ammonium persulfate as an oxidant”, *J. Mater. Chem. A*, vol. 2 (1), pp. 251-258, 2014.
85. Leung, A. C.; Hrapovic, S.; Lam, E.; Liu, Y.; Male, K. B.; Mahmoud, K. A.; Luong, J. H.; “Characteristics and properties of carboxylated cellulose nanocrystals prepared from a novel one-step procedure”, *Small*, vol. 7(3), pp. 302-305, 2011.
86. Saito, T.; Isogai, A.; “TEMPO-mediated oxidation of native cellulose. The effect of oxidation conditions on chemical and crystal structures of the water-insoluble fractions”, *Macromol.*, vol. 5 (5), pp. 1983-1989, 2004.
87. Batmaz, R.; Mohammed, N.; Zaman, M.; Minhas, G.; Berry, R. M.; Tam, K. C.; “Cellulose nanocrystals as promising adsorbents for the removal of cationic dyes”, *Cellulose*, vol. 21 (3), pp. 1655-1665, 2014.
88. Chan, C. H.; Chia, C. H.; Zakaria, S.; Sajab, M. S.; Chin, S. X.; “Cellulose nanofibrils: a rapid adsorbent for the removal of methylene blue”, *RSC Adv.*, vol. 5 (24), pp. 18204-18212, 2015.

# Chapter 2

## Experimental

## 2.1 Materials and instruments

### 2.1.1 Chemicals and reagents

The chemicals and reagents used in this research were analytical grade and used without further purification. Distilled water was used as solvent to prepare most of the solutions of this work. The chemicals and reagents which were used in this research are given below:

- i. Ethanol (Merck, Germany)
- ii. Toluene (Merck, Germany)
- iii. Sodium chlorite (BDH)
- iv. Sodium hydroxide (Merck, Germany)
- v. Sodium hypochlorite (Merck, Germany)
- vi. Sodium bromide (Loba, India)
- vii. Potassium hydroxide (Merck, India)
- viii. Potassium per sulfate (BDH)
- ix. Sulfuric acid (Merck, Germany)
- x. Hydrochloric acid (analytical grade)
- xi. 2,2,6,6-Tetramethylpiperidine-1-oxyl (TEMPO)
- xii. Acetone (analytical grade)
- xiii. Ferrous chloride  $4\text{H}_2\text{O}$ (Sigma Aldrich)
- xiv. Ferric chloride  $6\text{H}_2\text{O}$ (Sigma Aldrich)
- xv. Ammonia solution (25%)
- xvi. Tetraethylorthosilicate (TEOS) (Sigma Aldrich)
- xvii. 3-aminopropyltriethoxysilane (APTES) (Sigma Aldrich)

- xviii. N,N'-diethylformamide (DMF) (Merck, Germany)
- xix. Methacrylic anhydride (Sigma Aldrich)
- xx. Acrylic acid (BDH)

### 2.1.2 Instruments

Analysis of the samples was performed using the following instruments:

- i. Fourier Transform Infrared Spectrophotometer (SHIMADZU FTIR-8400)
- ii. Field Emission Scanning Electron Microscopy (JSM-7600F, Tokyo, Japan)
- iii. X-ray Diffractometer (Philips, Expert Pro, Holland)
- iv. X-ray photoelectron Spectroscopy
- v. Thermogravimetric analyser (TGA 50-H)
- vi. Centrifuge machine (Hettich, Universal 16A)
- vii. pH meter (Hanna, HI 8424, Romania)
- viii. Digital Balance (AB 265/S/SACT METTLER, Toletto, Switzerland)
- ix. Conductometer
- x. Freeze dryer (Heto FD3)

## 2.2 Fabrication of a novel magnetic nanocomposite

### 2.2.1 Extraction of Cellulose Nanocrystal (CNC)

Cellulose nanocrystals (CNCs) from environmental waste sawdust were prepared by acid hydrolysis of the cellulose which has already established in our lab [1]. Briefly, sawdust was firstly dried at 85 °C for 4h and then dewaxed in soxhlet apparatus with 2:1 (v/v) mixture of toluene and ethanol at 150 °C for 6 hours. After that, delignification was carried out using an acidified sodium chlorite solution at 75 °C for 1 hour and repeated six to seven times until

products become white. Next, blended product was treated with 5% KOH at 90 °C for 2h. This process was also repeated more than 2 times and got chemically purified cellulose. This chemically purified cellulose was further blended 10 min and then subjected to acid hydrolysis using concentrated sulfuric acid (64%) to get cellulose nanocrystal. The reaction was carried out at 45 °C under vigorous mechanical stirring for 60 min. The hydrolysis reaction was terminated after 60 min by placing the product in an ice cool water bath. The suspension was then washed with distilled water and centrifuged at 4000 rpm for 15 min.

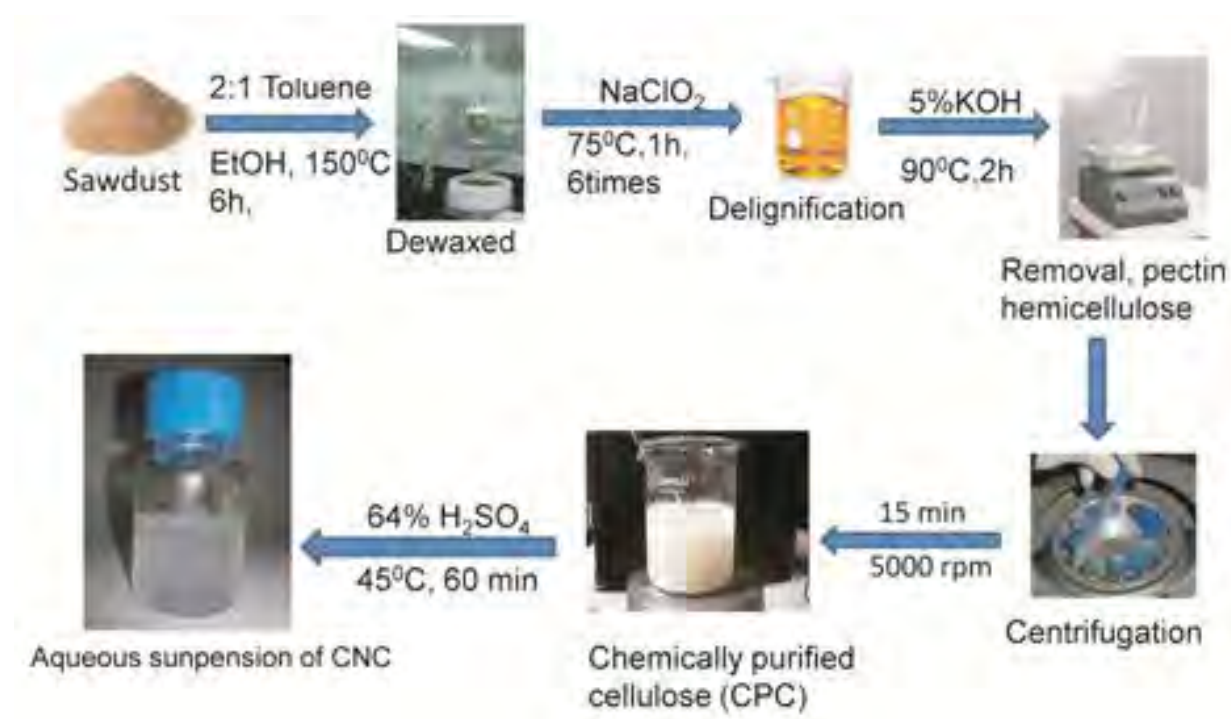


Figure 2.1 Schematic representation of extraction of cellulose nanocrystal from sawdust.

The centrifugation process was repeated until constant pH was obtained. It was then placed into dialysis tube and dialyzed against distilled water until pH was neutral (pH 6 -7). After this dialysis process the suspension was again centrifuged at 4000 rpm for 15 min followed by sonication for 10 min in ice bath. Then the resultant concentrated aqueous suspension of cellulose nanocrystals was stored in refrigerator at 4 °C for further use.

### 2.2.2 Synthesis of carboxylated cellulose nanocrystals (CCN)

The primary hydroxyl groups on the surface of CNC were oxidized to carboxyl groups using TEMPO-reagent in the presence of sodium bromide (NaBr) and sodium hypochlorite



(NaClO). The reaction conditions were adjusted by the previous studies [2, 3, 4]. 1g CNC was dispersed in 100 mL distilled water. After mixing, sonication was performed for 10 min in ice bath to get a homogeneous dispersion of CNC. 16 mg TEMPO and 100 mg NaBr was weighed and dissolved separately. After that mixed with CNC suspension and stirred 10 min at room temperature.

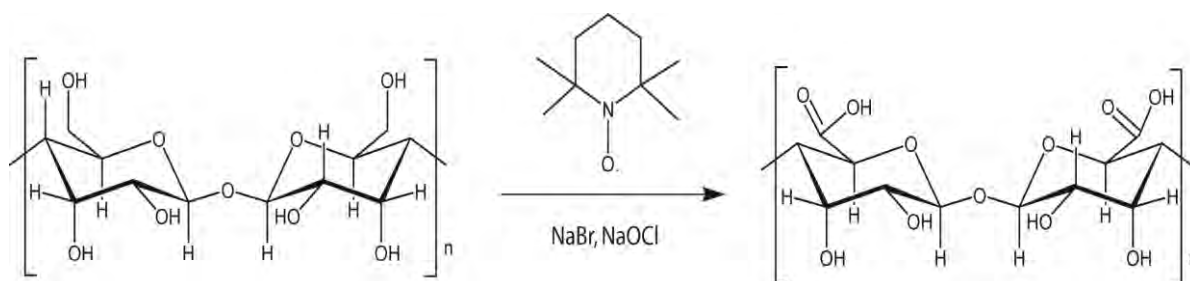


Figure 2.2 Schematic representation of carboxylated cellulose nanocrystals

This was further sonicated for 15min. The oxidation was initiated with the addition of 3.5 mL of 4-14% NaClO solution to the CNC suspension by dropwise. The pH of the solution was maintained constant at 10 by adding 0.1M NaOH solution until no more variation was observed, indicating that the reaction was finished. Then the solution was continuously stirred for 12 h. Finally, 5 mL of ethanol was added to stop the oxidation. Then the solution was washed with distilled water several times and finally obtained concentrated suspension which was sonicated for 2 min and stored at 4 °C.

### 2.2.3 Synthesis of acrylated magnetic iron oxide nanoparticles

The magnetite iron oxide nanoparticles (MION) were prepared by the most common, easy and widely used, chemical co-precipitation method [5]. Firstly, an iron salt solution was obtained by mixing 0.005 mol 2.703g FeCl<sub>3</sub> and 0.0025 mol 0.6336g FeCl<sub>2</sub> such that the ratio of Fe<sup>3+</sup> to Fe<sup>2+</sup> becomes 2 in 50 mL distilled water which is deoxygenated by passing N<sub>2</sub> gas about 10 min. 20 mL of 1.5M NaOH was rapidly poured into the iron salt solution under vigorous magnetic stirring at room temperature (RT). Orange color of the iron salt solution was instantly changed and black precipitate was found. After continuously stirring for 20 min, the precipitate was separated magnetically and then washed with distilled water for several times by centrifugation. Next, magnetic iron oxide nanoparticles (MION) were coated with silica by hydrolysis of tetraethylorthosilicate (TEOS) in basic solution via Stöber's

method [6]. In this case, 300 mg magnetite nanoparticles were dispersed into a mixture of 240 mL ethanol and 60 mL distilled water and sonicated for 15 min. The pH value was adjusted to 9 with 25% ammonia solution and 4 mL TEOS was added under vigorous stirring. The resulting dispersion was mechanically stirred for 10 hour at room temperature. For complete hydrolysis, the sample was heated at 50 °C for 12 hour. After cooling the sample, solvent was removed by centrifugation, and then the sample was washed with anhydrous ethanol and later washed with dimethyl formamide (DMF). After that, DMF washed silica-coated MION were ultrasonically redispersed into a solution containing 120 mL DMF and 80 mL toluene, then taken into a double-necked RB flask. 10 mL (3-aminopropyl) triethoxysilane (APTES) was added dropwise under magnetic stirring. After hydrolysis for 24 h at room temperature, the particles were separated by centrifugation and washed with toluene several times. The sample was then taken into 250 mL RB flask containing 150 mL toluene and heated at 120 °C until the sample volume became 90 mL. After reaching that volume heating stopped and kept for cool down at room temperature. Always covered the flask tightly because water absorbed by the sample. After that 6.7 mL methacrylic anhydride was added to the sample and magnetically stirred about 4 hours. Finally, the sample was washed with toluene several times and kept in toluene and got acrylic modified magnetic iron oxide nanoparticles. It is very essential to keep the sample into water for future reaction. For this solvent exchange needed from toluene to water. Toluene and water are practically insoluble in each other. Toluene and acetone are miscible in all proportions, as are also acetone and water. For this reason acetone was added to sample in toluene and after that solvent was removed. This was repeated several times and as a result toluene was almost completely removed. After that, water was added to the sample in acetone. This was repeated several times and the sample was heated at 58 °C. As a result, acetone was completely removed and the sample retained in water.

#### 2.2.4 Synthesis of nanocomposite

PAA/Fe<sub>3</sub>O<sub>4</sub>/CCN nanocomposite was synthesized via in *situ* polymerization process. 36 mg of CCN and 14 mg of acrylated MION was taken into a beaker individually containing 10 mL distilled water and sonicated for 5 min in an ice bath and the temperature kept below 20 °C. After that CCN and coated magnetic iron oxide was mixed and further sonicated for 15 min. 25 mg of potassium per sulfate (KPS) was taken into 5 mL distilled water and dissolved properly. 1 mL acrylic acid was added dropwise at 12 °C under sonication in ice bath. Finally

free radical polymerization was allowed to continue by adding KPS solution dropwise. This mixture was heated at 58 °C and continuously stirring at 1200 rpm for 4 hours. After completion of the reaction, resulting nanocomposite was washed with distilled water several times and dried with freeze dryer.

Magnetic as well as dispersive properties containing nanocomposite give high performing materials. For getting such nanocomposite, various amount of CCN, 3D crosslinker and acrylic acid were taken and optimized. The varied ratio of CCN, 3D crosslinker and acrylic acid which was performed are 1:0.2:40, 1:0.3:80, 1:0.4:30, 1:0.4:86, 1:0.4:110, 1:0.5:80, 1:1.25:200. The effect of temperature on the synthetic procedure also recorded. Moreover, a composite material also synthesized using 3D crosslinker and acrylic acid except CCN.

### **2.3 Conductometric titration**

The carboxyl content of cellulose nanocrystals was determined by conductometric titration. Typically 40 mg of TEMPO oxidized cellulose nanocrystals were suspended into 50 mL of distilled water. After 10 min stirring, titration was performed using 0.01M solution of NaOH (solution was standardized against oxalic acid) and the conductivity was monitored with a Mettler Toledo Conductivity meter USA).

### **2.4 Fourier transform infrared analysis (FTIR)**

The infrared spectra of the cellulose nanocrystal, carboxylated cellulose nanocrystal, magnetic iron oxide nanoparticle (MION), Silica coated MION, aminated MION, acrylated MION and nanocomposite samples were recorded on an FTIR spectrometer in the region of 4000 – 400  $\text{cm}^{-1}$ . A small portion of cellulose nanocrystal and carboxylated CNC (CCN) was taken into vial and oven dried at 80 °C. After that it was cut as much as possible small sized pieces and then grinded as much as possible. On the other hand magnetic iron oxide nanoparticles, silica coated magnetic iron oxide nanoparticles, aminated MION, acrylated MION were dried and grinded into a mortar with a pestle. The powder mixture was then compressed in a metal holder under a pressure of 8–10 tons to make a pellet. The pellet was then placed in the path of IR beam for measurements.

### **2.5 Field emission scanning electron microscopy (FE-SEM)**

The surface morphology of the synthesized CNC, CCN, magnetic iron oxide nanoparticles (MION), silica coated MION, aminated MION, acrylated MION, PAA/Fe<sub>3</sub>O<sub>4</sub>/CCN

nanocomposite was adopted using Field Emission Scanning Electron Microscopy (FE-SEM). Glass substrate was used for the sample preparation of MION, acrylated MION and nanocomposite. The concentration was 0.0001%. One drop of dilute sample was taken on the surface of glass and air dried. But in case of CNC and CCN, silicon substrate was used. 0.05% CNC and CCN was taken on the surface of silicon substrate and the freeze dried about 24 hour. The sample loaded substrate was then mounted to a chamber that evacuated to  $\sim 10^{-3}$  to  $10^{-4}$  tor and then a very thin platinum layer (few nanometers thick) were sputtered on the sample to ensure the conductivity of the sample surface. The sample was then placed in the main FE-SEM chamber to view its surface. The microscope was operated at an accelerating voltage of 5.0 kV.

### **2.6 Energy dispersive x-ray (EDX) spectra**

Elemental analyses of the synthesized CNC, CCN, MION, silica coated MION, acrylated MION, nanocomposite were performed by EDX spectra. The dried powders of CNC, CCN & magnetic iron oxide nanoparticles based nanocomposite were placed on a 1 cm  $\times$  1 cm conducting steel plate. The steel plate was then placed on a conducting carbon glued strip. The sample was then placed in the main FE-SEM chamber integrated with the EDX instrument.

### **2.7 X-ray diffraction (XRD)**

The crystallinity of magnetic iron oxide nanoparticles and nanocomposite were analyzed by X-ray diffraction pattern in the powder state. The powder samples were pressed in a square aluminum sample holder (40 mm  $\times$  40 mm) with a 1 mm deep rectangular hole (20 mm  $\times$  15 mm) and pressed against an optical smooth glass plate. The upper surface of the sample was labeled in the plane with its sample holder. The sample holder was then placed in the diffractometer.

### **2.8 X-ray photoelectron spectroscopy (XPS)**

XPS measurements were performed on samples that had been prepared within 4 days using the AXIS ULTRA spectrometer (Kratos Analytical). The base pressure in the analytical chamber was  $<3 \times 10^{-8}$  Pa. The monochromatic AlK $\alpha$  source ( $h\nu=1486.6\text{eV}$ ) was used at a power of 210 W. The photoelectron exit angle was  $90^\circ$ , and the incident angle was  $35.3^\circ$  from the plane of the surface. The analysis spot was 400  $\times$  700 $\mu\text{m}$ . Survey scans were

collected for binding energies from 1100 to 0eV with analyzer pass energy of 160eV and a step of 0.35eV. The high-resolution spectra were run with a pass-energy of 20eV and a step of 0.1eV. Relative sensitivity factors (RSFs) for different elements were as follows: 1 for C (1s), 1.8 for N (1s), 2.93 for O (1s), 0.26 for Si (2s), 0.27 for Si (2p). Only one set of XPS scans was performed on a given sample; therefore, XPS analysis before and after surface reactions were performed on different samples.

### **2.9 Thermogravimetric analysis (TGA)**

The thermal stability of CCN, acrylated MION, nanocomposite and 3D crosslinked poly(acrylic acid) were studied by a thermo-gravimetric analyzer (TGA) in a nitrogen atmosphere. Approximately 3-10mg freeze dried samples taken into an aluminum cell and heated from 30 to 800 °C at a heating rate of 10 °C/min under a nitrogen flow of 10 mL/ min. Before the data acquisition segment, the sample was equilibrated at 25 °C for 5 min to obtain an isothermal condition.

## References

1. Kumar, A.; Negi, Y. S.; Choudhary, V.; Bhardwaj, N. K.; “Characterization of cellulose nanocrystals produced by acid hydrolysis from sugarcane bagasse as agro-waste”, *J. Mater. Physic. Chem.*, vol. 2 (1), pp. 1-8, 2014.
2. Saito, T.; Isogai, A.; “Cellulose nanofibers prepared by TEMPO-mediated oxidation of native cellulose”, *Biomacromol.*, vol. 8, pp. 2485-2491, 2007.
3. Habibi, Y.; Chanzy, H.; Vignon, M. R.; “Optimization of cellouronic acid synthesis by TEMPO-mediated oxidation of cellulose III from sugar beet pulpCellulose”, vol. 13, pp. 679, 2006.
4. Saito, T.; Isogai, A.; “TEMPO-mediated oxidation of native cellulose. The effect of oxidation conditions on chemical and crystal structures of the water-insoluble fractions”, *Biomacromol.*, vol. 5, pp. 1983-1989, 2004.
5. He, Y. P.; Wang, S. Q.; Li, C. R.; Miao, Y. M.; Wu, Z. Y.; Zou, B. S.; “Synthesis and characterization of functionalized silica-coated Fe<sub>3</sub>O<sub>4</sub> superparamagnetic nanocrystals for biological applications”, *J. Physics D: Appl. Physic.*, vol. 38, pp. 1342–1350, 2005.
6. Nedkov, I.; Merodiiska, T.; Slavov, L.; Vandenberghe, R. E.; Kusano, Y.; Takada, J.; *J. Magn. Magn. Mater.*, vol. 300 (2), pp. 358–367, 2006.

# Chapter 3

## Results and Discussion

### 3.1 Fabrication of magnetic nanocomposite

#### 3.1.1 Synthesis of carboxylated cellulose nanocrystals (CCN)

Cellulose nanocrystals (CNC) were synthesized from sawdust. Sawdust is cheap, easily available and a new source of CNC. This environmental waste material used as cheap fuel source. So for environmental safety and also for industrial purposes, CNCs extraction from sawdust creates a new dimension. CNC extracted from sawdust by acid hydrolysis process [1]. Before acid hydrolysis sawdust was pretreatment with different chemicals. The mixture of toluene and ethanol was used for the complete removal of waxy materials. Acidified sodium chlorite was used several times for the taking away of lignin, pectin and hemicelluloses. pH was maintained almost neutral by centrifugation for the acid hydrolysis. Chemically purified cellulose contains both amorphous and crystalline region. Acid hydrolysis was carried out to get crystalline region. During acid hydrolysis, the hydronium ions cleaved the glycosidic linkages and thereby releasing the individual crystallites. This crystallite is known as CNC which contain negatively charged surface due to the presence of sulfate group. CNC is highly dispersive in most of the solvent. A wide range of hydroxyl groups on the surface of CNC are responsible for the tightly hydrogen bonded networks. To loosen the hydrogen bond, increase the electrostatic repulsion and adsorption ability, primary hydroxyl group of CNC was converted to carboxyl group and this carboxyl group containing CNC known as carboxylated cellulose nanocrystal (CCN). This converting was carried out by 2, 2, 6, 6-tetramethylpyperidine-1-oxyl (TEMPO) mediated oxidation. In this process TEMPO was used as primary oxidant and sodium hypochlorite was as secondary oxidant. During this process NaBr was used to increase the rate of oxidation through the formation of sodium hypobromite. At  $\text{pH} < 8$  the reaction proceeds slowly and selectivity between primary and secondary alcohols was not as prominent as at  $9 < \text{pH} < 11$  where the reaction showed good selectivity to primary alcohol.



The mechanism of TEMPO mediated oxidation of CNCs is shown in figure 3.1.

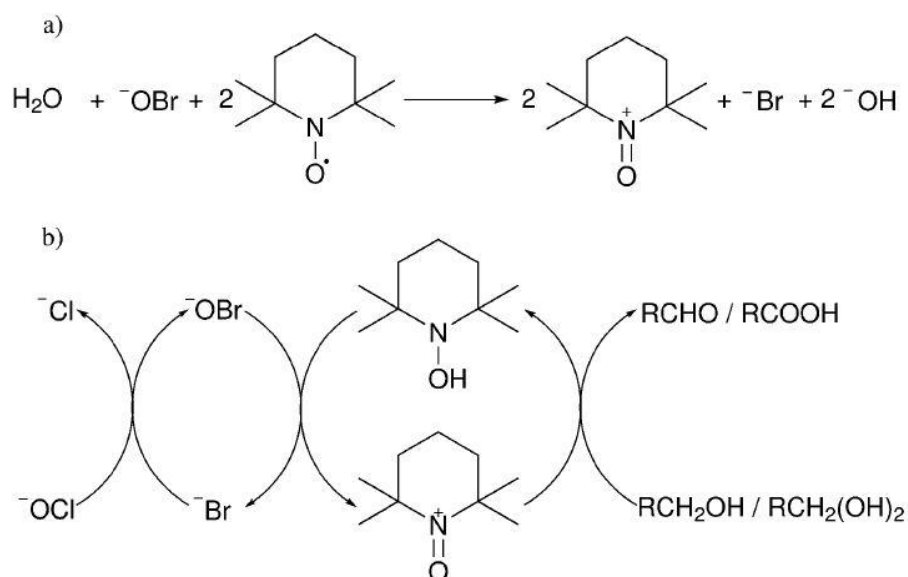


Figure 3.1 Mechanism of TEMPO mediated oxidation (a) initial formation of oxidant from TEMPO radical and (b) catalytic cycle of TEMPO oxidation.

CCN is better adsorbent over CNC due to the presence of carboxyl group. It may act as better nanofiller in nanocomposite.

### 3.1.2 Synthesis of 3D crosslinker

For linking one polymer chain to another polymer chain crosslinker plays a vital role. Some crosslinkers are commercially available and some are lab prepared. Among different crosslinkers 3D crosslinker has comparatively larger surface area and reactive sites than conventional linear or planar crosslinker. In this research a high performance 3D crosslinker was developed. This type of 3D crosslinker contained both magnetic and acrylic group which was able to link with polymer chain. For magnetic property magnetic iron oxide nanoparticles (MION) were synthesized via chemical co-precipitation method. This reaction was carried out using deoxygenated water by passing  $\text{N}_2$  gas so that produced magnetic iron oxide nanoparticles could not come in contact with air. If these nanoparticles come in contact with air, it oxidized to  $\text{Fe}_2\text{O}_3$ . As a result, the amount of  $\text{Fe}_3\text{O}_4$  decrease and impurity incorporate which affect the further treatment. For this reason coating of nanoparticles is very essential and this urgent work was done by coating with silica using tetraethylorthosilicate (TEOS) in basic medium (25%  $\text{NH}_3$  solution). In aqueous medium polymer of silica was formed very rapidly. Anhydrous ethanol was used for controlling the reaction and for this case two step reactions was carried out. First step, after addition of TEOS stirred 10 hour without heat.

Next step was carried out applying heat for 12 hours so that Si-O-Si bond break down and form Si-OH on the surface of MION and completely coated.

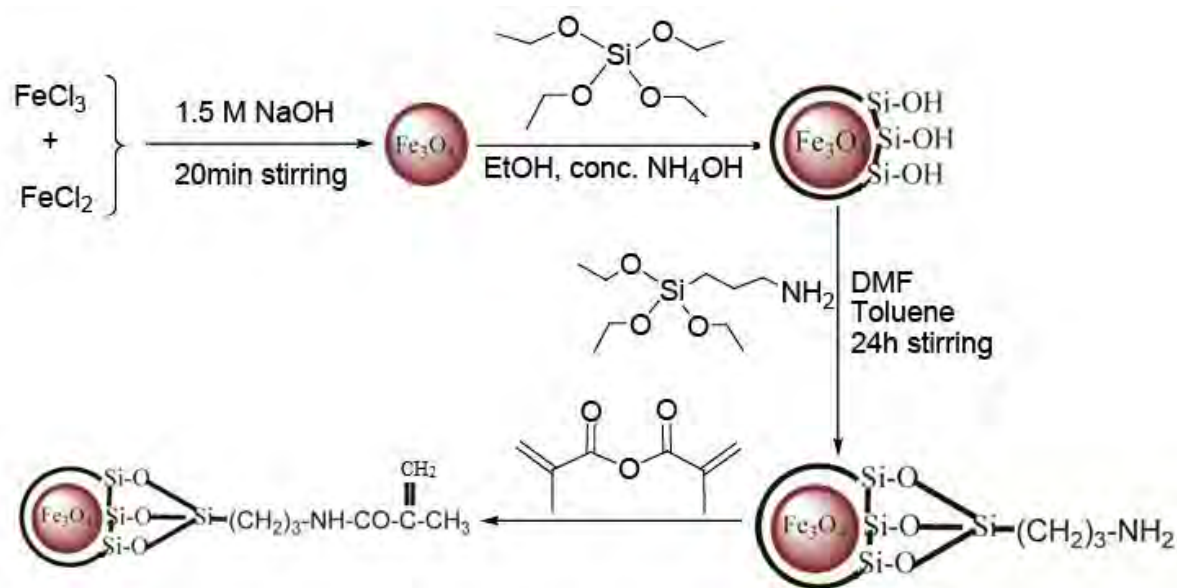


Figure 3.2: Schematic representation of 3D crosslinker synthesis

Silica coated MION was functionalized by amino group for the further treatment with methacrylic anhydride. The amino group of the aminated MION and the anhydride group of the methacrylic anhydride formed amide bond. This was also contained acrylic group at the end of the chain. Acrylic group was capable to link directly with polymer chain.

### 3.1.3 Nanocomposite synthesis

For the synthesis of nanocomposite, CCN and 3D crosslinker were sonicated so that the aggregated particles apart from each other. The mixing procedure was carried out with in sonicator in an ice bath below 20 °C. The mixture of CCN and 3D crosslinker was sonicated long time and that time acrylic acid was added because the dispersion of acrylic acid was occurred homogenously. During sonication dissolved potassium per sulfate (KPS) which was used as initiator, was added rapidly so that polymerization undergoes very rapidly.

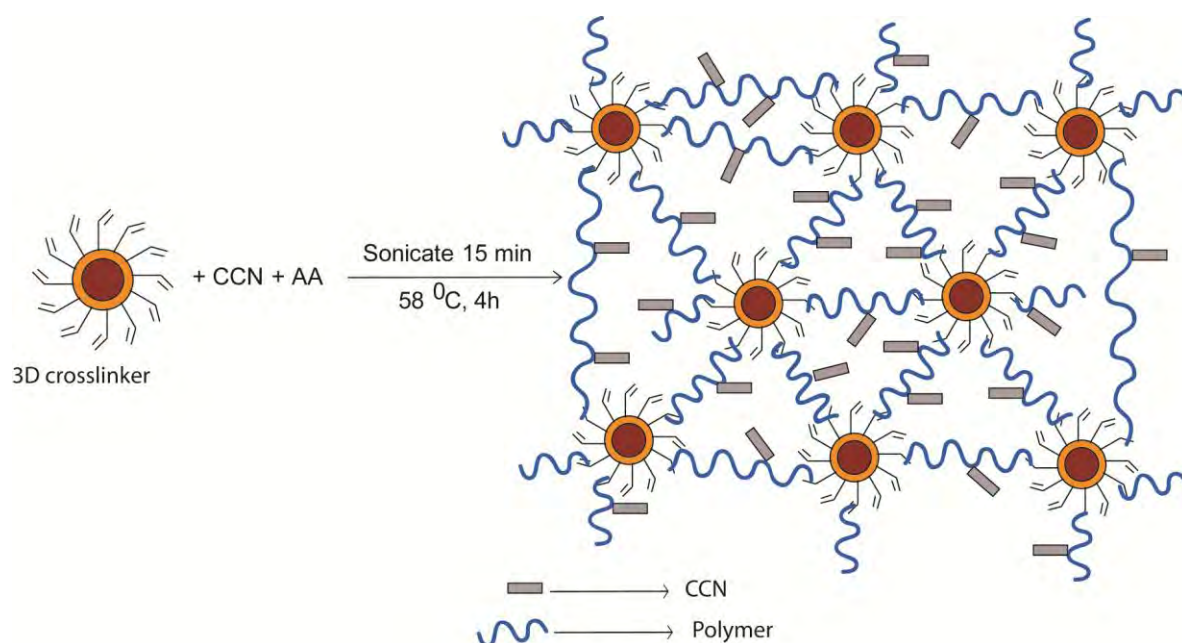


Figure 3.3 Schematic representation of nanocomposite synthesis

Highly reactive sites of 3D crosslinker are able to link with many more polymer chains. As a result, composite became very sticky and adhesive. When this type of composite was used as adsorbent, they were settled down and adsorption was not much significant. So their adhesiveness needs to decrease and increase the dispersiveness. CCN was used to decrease the adhesive property of the composite materials and increase the dispersive property. At higher amount of CCN and lower amount of 3D crosslinker produced composite was dispersive but not magnetic and the reverse the composite was highly adhesive. So optimize the better condition of the synthesis of nanocomposite. For this purpose different ratio of CCN, 3D crosslinker and acrylic acid (AA) and the optical images of the synthesized nanocomposites are given in the figure 3.4. Image A is for 3D crosslinked poly(acrylic acid) which did not contain any CCN. This composite was very sticky and adhesive. It was not dispersive and also non magnetic. Image B contains CCN. As a result the adhesive property decreased and the composite materials become dispersive but the magnetic property was not noticeable. It may cause comparatively small amount of 3D crosslinker compared to CCN. Image C contained more 3D crosslinker than image B. But in this case the composite becomes hard. When dried it acts as hydrogel. This composite was not dispersive and did not show magnetic property. A dramatic change occurs in image D when the ratio of CCN, 3D crosslinker and acrylic acid was taken 1: 0.4: 30.

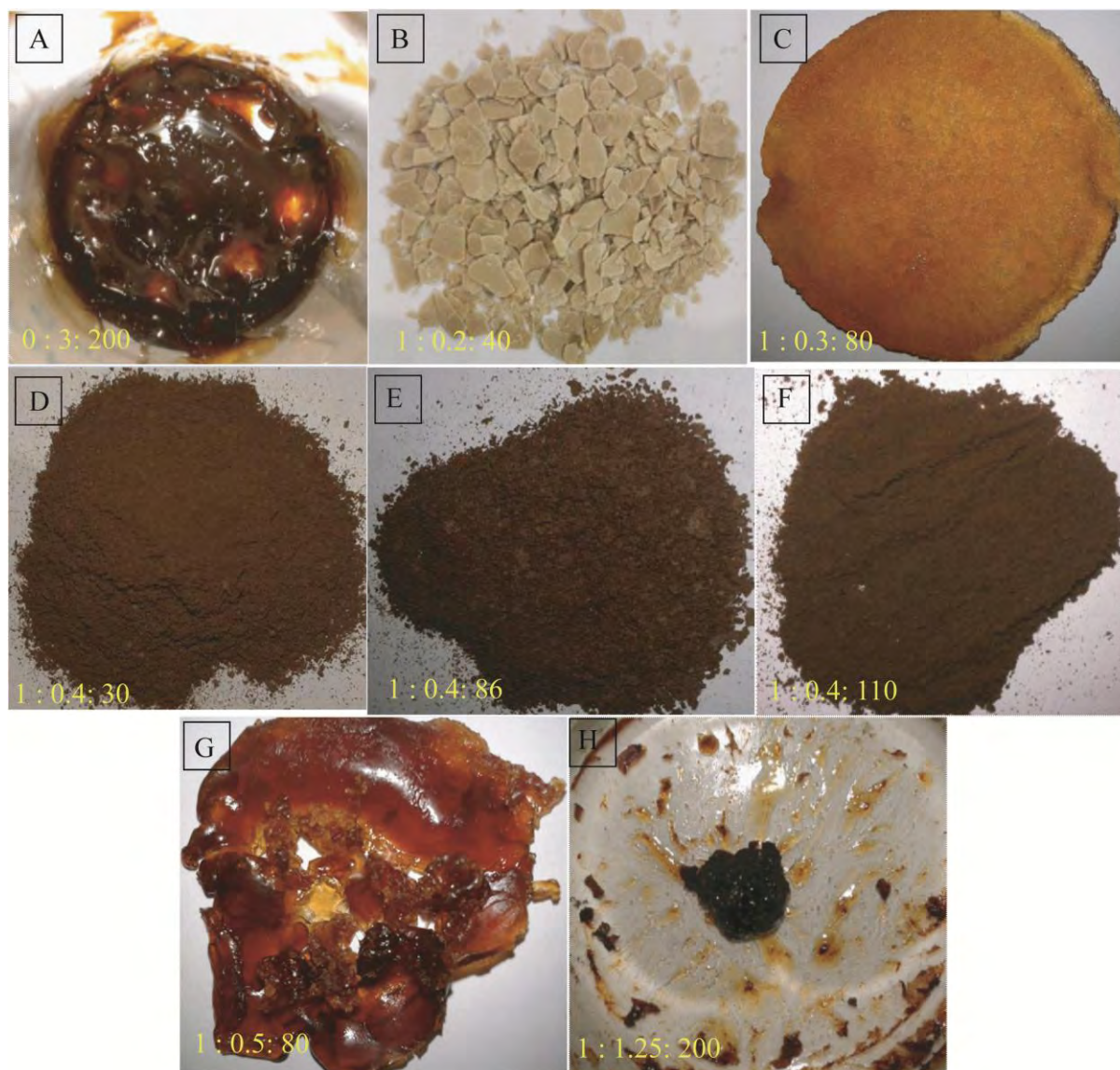


Figure 3.4 Different ratio of CCN, 3D crosslinker and acrylic acid in nanocomposite

The composite was dispersive and showed magnetic property. This composite was powder like. Image E and F where the amount of CCN and 3D crosslinker remain same but the amount of acrylic acid was varied. Both the composites were highly dispersive and also magnetic. It may say that for this composite there was no impact of acrylic acid in low or high amount. Image G and H where the amount of 3D crosslinker increased but the composite become sticky and adhesive. Both the composites were not dispersive and non magnetic. The ratio of CCN, 3D crosslinker and acrylic acid 1: 0.4:30, 1: 0.4: 86, 1:0.4: 110 are the better condition for the synthesis of nanocomposite. The effect of temperature also observed. The composite materials become very adhesive and sticky when the nanocomposite was synthesized at the temperature upper than 60 °C like 70 °C, 75 °C. At higher temperature



the rate of polymerization increases and the 3D crosslinkers may polymerize itself and form crosslinker polymer chain. As a result, polymer chains get together and become sticky and adhesive. The best condition of the synthesis of nanocomposite was 58 °C.

### 3.2 Magnetic test of nanocompoiste

The magnetic test of the synthesized nanocomposite was carried out using magnetic bar. If the particles are magnetic then they are attracted by magnet and if the particles are not magnetic they are not attracted by the magnet. This test was performed two states like when the particles were dispersed in water and when the particles were dried. In the first case, the particles of nanocomposite were highly dispersed in water but when a magnetic bar took to the vial then the particles were attracted by the magnetic bar. It was also seen when the nanoparticles were dried. So from this test it may say that synthesized nanocomposite was magnetic.

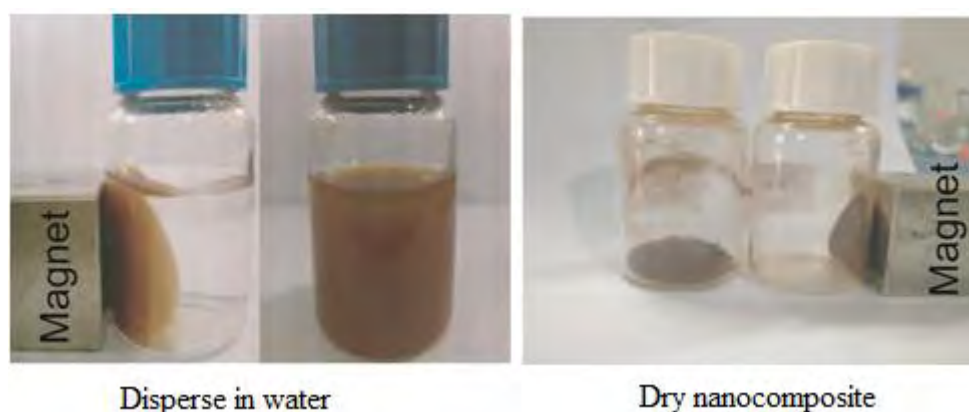


Figure 3.5 Magnetic test of synthesized nanocomposite

### 3.3 Functional group analysis using FTIR

In order to confirm that the presence of functional groups on the surface of CNC and chemically modified CNC, FTIR spectra of the samples were investigated. Figure 3.6 shows the FTIR spectra of CNC, CCN and nanocomposite.

First one is for CNC, the second one for CCN, and third one for nanocomposite. The broad peak between  $3600\text{ cm}^{-1}$  and  $3400\text{ cm}^{-1}$  in the spectra both of CNC & CCN is due to the presence of O-H stretching vibrations.  $850\text{-}1500\text{ cm}^{-1}$  region is sensitive to crystal structure of the cellulosic material. Spectral bands at  $1420\text{-}1430\text{ cm}^{-1}$  and  $893\text{-}897\text{ cm}^{-1}$  are very important to elucidate to the crystal structure of cellulosic material [1]. The peaks at 1163 and

$1070\text{ cm}^{-1}$  are related to the saccharides structure [2] and the peak at  $1250\text{ cm}^{-1}$  asymmetrical S=O vibration which shows the presence of sulfate ester groups on the surface of CNC [3]. Other characteristic peaks of CNC that are found in our study are shown in table 3.1.

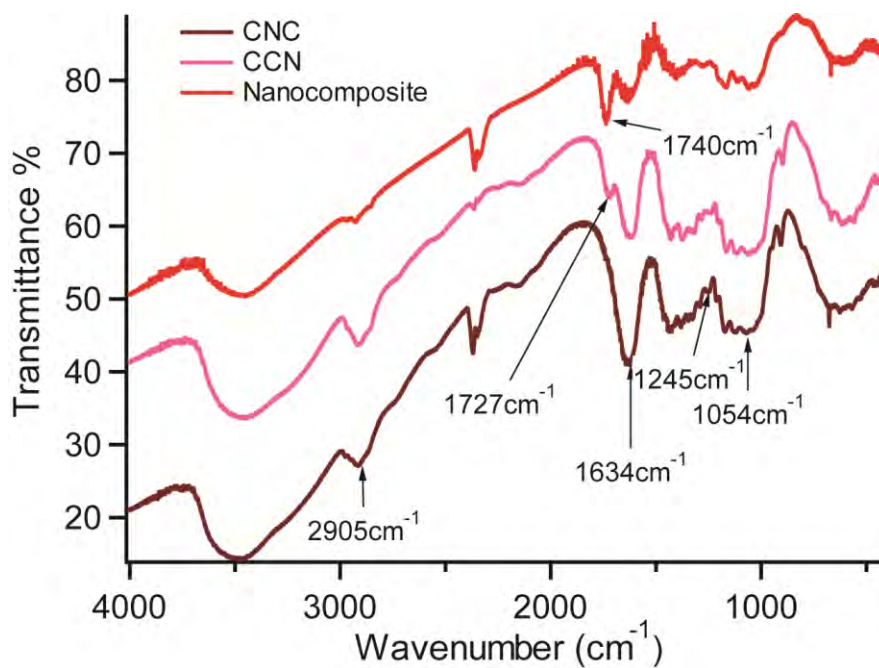


Figure 3.6 FTIR spectra of CNC, CCN and nanocomposite

Table 3.1 Characteristic IR bands of CNC, CCN and nanocomposite

Wavenumber ( $\text{cm}^{-1}$ )	Interpretation
2905	C-H stretching
2360	$\text{sp}^3$ C-H stretching
1634	for water adsorption from air by cellulose materials
1422	C-H bending
1377	C-H bending
1317	$\text{CH}_2$ wagging
1245	C-O out of plane stretching
1110	C-O-C glycosidic ether band
1054	C-O-C pyranose ring stretching vibration
898	$-\text{CH}_2$ bending

The second peak is for carboxylated CNC. The FTIR spectrum of the CCN was compared with the spectra of CNC, where the appearance of a new peak at  $1728\text{ cm}^{-1}$  corresponds to the carboxyl group, which validates the oxidation process [4]. The 3<sup>rd</sup> one is for nanocomposite. Here is found a new peak at  $1740\text{ cm}^{-1}$  which is for C=O group.

Figure 3.7 shows the FTIR spectra of magnetic iron oxide nanoparticles (MION) and modified MION. The 1<sup>st</sup> one is for MION. The strong absorption peak at  $578\text{ cm}^{-1}$  attribute to the vibration of Fe-O bond and this is the characteristic peak of bare  $\text{Fe}_3\text{O}_4$ . This also indicates the  $M_{\text{tetrahedral}}$  resonance with oxygen. The peak at  $1627\text{ cm}^{-1}$  indicates the presence of O-H vibration in  $\text{H}_2\text{O}$  and the peak at  $3425\text{ cm}^{-1}$  is attributed to the stretching vibrations of OH adsorbed on the surface of the  $\text{Fe}_3\text{O}_4$  nanoparticle. The 2<sup>nd</sup> one is for silica coated MION. The strong peaks at  $1080\text{ cm}^{-1}$  and  $804\text{ cm}^{-1}$  have been assigned to the asymmetric and symmetric linear stretching vibrations of Si-O-Si bonding. The bending vibration absorption peaks of Si-O-Si and Si-OH were observed at  $461\text{ cm}^{-1}$  and  $962\text{ cm}^{-1}$  respectively. These indicates that the successfully coating of silica layer on the surface of magnetic iron oxide nanoparticles.

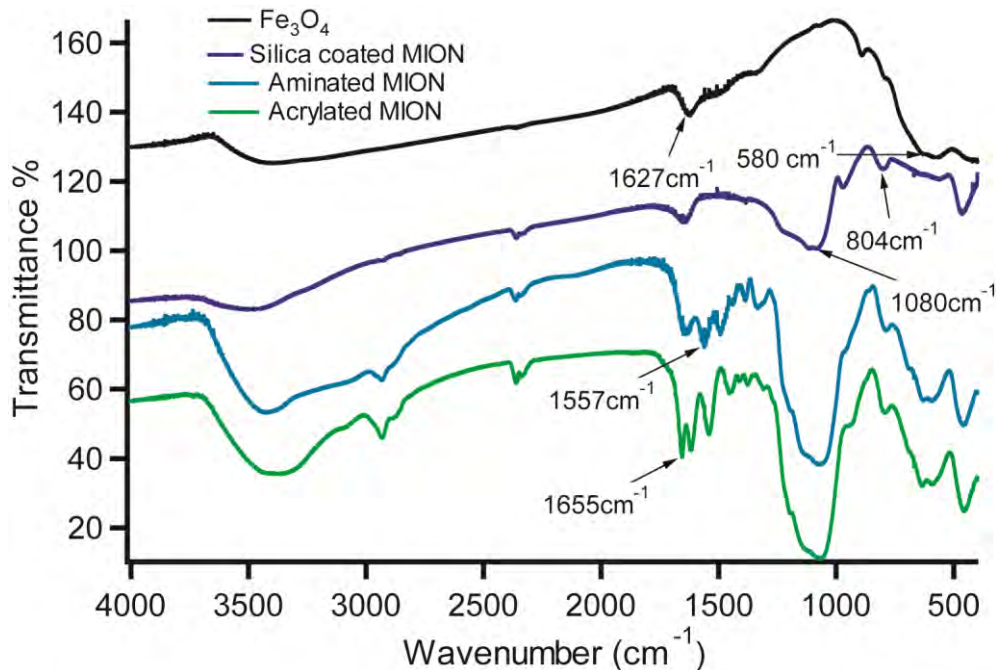


Figure 3.7 FTIR spectra of  $\text{Fe}_3\text{O}_4$ , silica coated MION, aminated MION and acrylated MION

In the spectrum of aminated MION, the two bands at  $3422\text{ cm}^{-1}$  and  $1650\text{ cm}^{-1}$  can be referred to the N-H stretching vibration and  $\text{NH}_2$  bending mode of free  $\text{NH}_2$  group, respectively [5]. The anti symmetric C-H stretching vibrations appeared at  $2935\text{ cm}^{-1}$ , and the

bending vibration absorption peaks of  $-CH_2$  and  $-CH_3$  appeared in  $1492\text{ cm}^{-1}$  and  $1385\text{ cm}^{-1}$ , respectively; The C-N stretching vibrations appeared at  $1335\text{ cm}^{-1}$ . The deformation vibration absorption peak of N-H appeared at  $1553\text{ cm}^{-1}$ . These indicate the successful introduction of APTES to the surface of silica coated magnetic NPs. The 4<sup>th</sup> one is for acrylated MION. The sharp peak at  $1655\text{ cm}^{-1}$  is the characteristic peak of C=C bond. From this it may say that the vinyl group was successfully added to the aminated MION.

### 3.4.1 X-ray photoelectron spectroscopy (XPS)

In order to assess and confirm the bonds that were formed in aminated MION, acrylated MION and nanocomposite, were characterized by X-ray photoelectron spectroscopy.

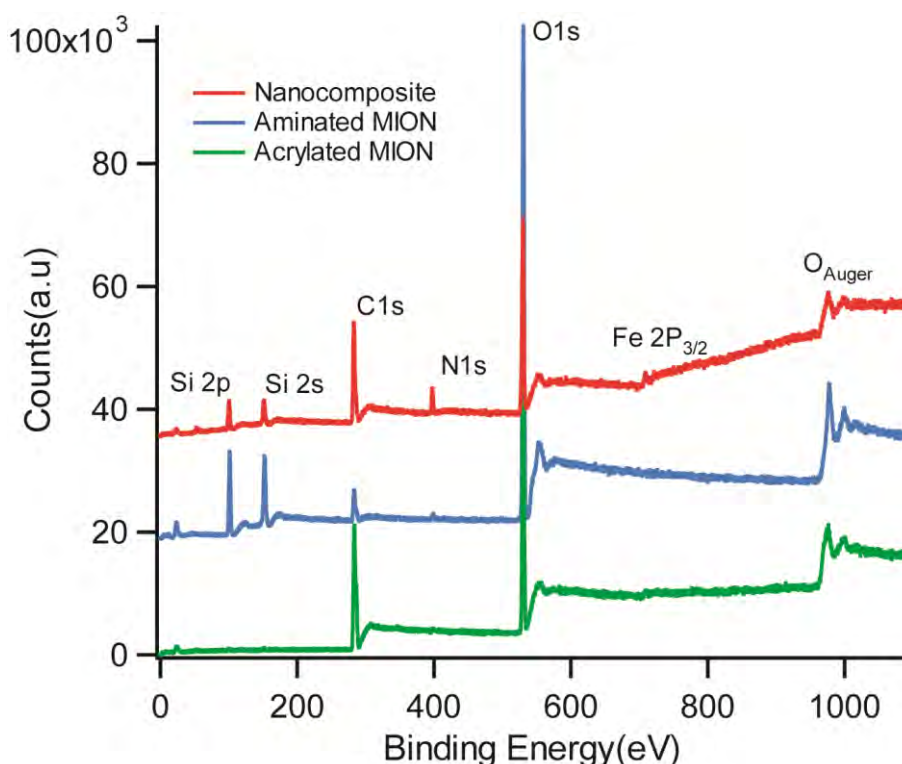


Figure 3.8 Widescan spectra of aminated MION, acrylated MION and nanocomposite

The widescan XPS spectra of aminated MION, acrylated MION and nanocomposite is shown in figure 3.8. Widescan spectra give idea about the elemental composition present on the surface. But their bonding nature could not be known by this spectrum. From the figure 3.8 the widescan spectra of all the samples are similar because there is no elemental change occurred during acrylation or in the formation of nanocomposite. All XPS spectra reveal the presence of C1s, O1s, N1s, Si2s, Si2p. The spectrum of aminated MION ascribe the



dominant species are O and Si. But in case of aminated MION and nanocomposite the dominant species are O and C. the intensity of N1s very small in aminated and acrylated MION but significant in nanocomposite. The predominating species C and O are found at the binding energy 283.6 eV and  $\sim$ 532.8 eV, respectively. The presence of nitrogen on the surface was detected from its characteristic emission peak at  $\sim$ 400 eV and is due to the amination of silica coated MION and amide formation in acrylated MION and also in nanocomposite. The binding energy at 100.4 eV and 151.2 eV reveals the existence of silicon on the surface as the magnetic iron oxide nanoparticles were coated with silica. All the three spectra have a common oxygen auger electron spectrum at binding energy 978 eV.

### 3.4.2 High Resolution C1s Spectra

Widescan spectra showed the presence of C but the relation of C with other elements could not explain. For this high resolution of C1s spectra were taken. By this spectrum it is possible to know how the C bonded with other elements. High resolution C1s spectra of aminated MION, acrylated MION and nanocomposite are shown in figure 3.9.

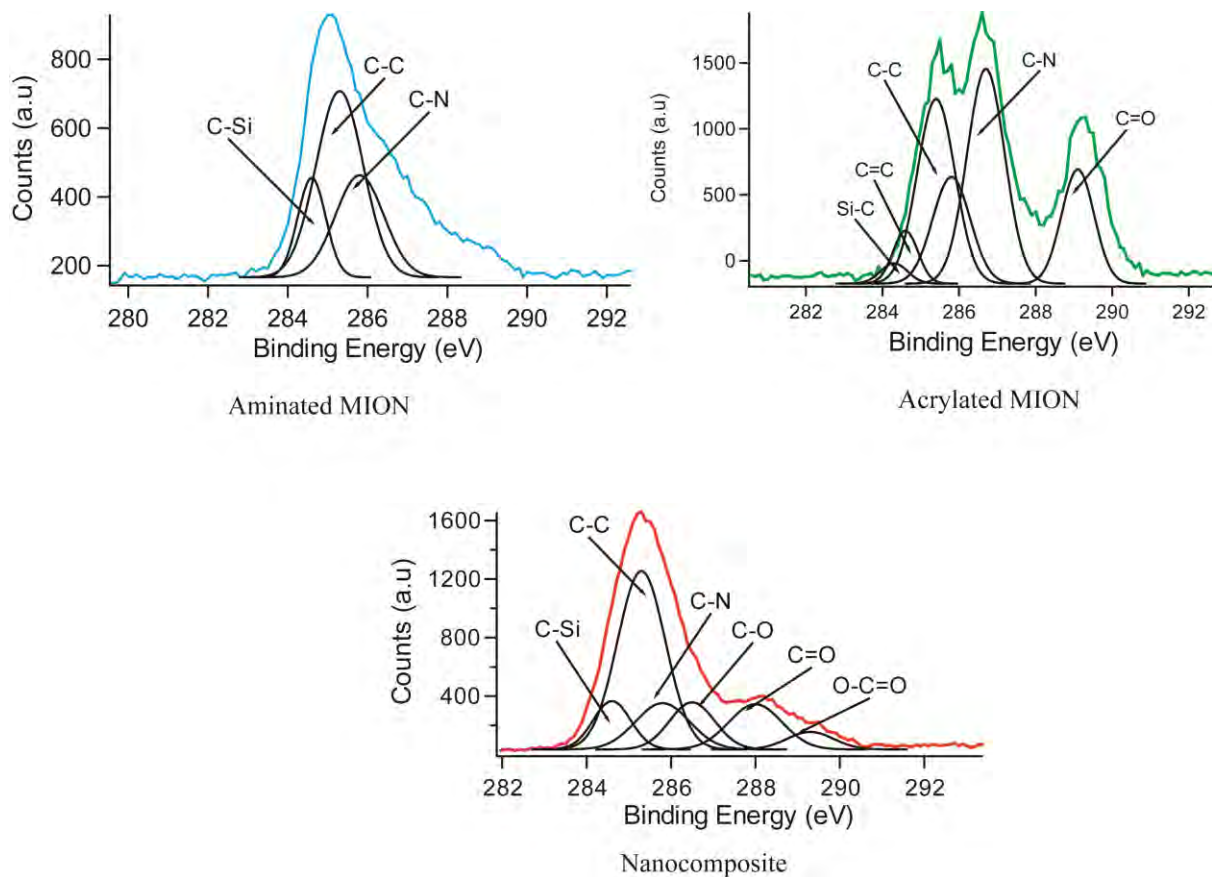


Figure 3.9 High resolution of C1s spectra of aminated MION, acrylated MION and nanocomposite

The C1s peak of aminated MION can be deconvoluted into three components peak. According to the binding energy these peaks are assigned to the carbon of C-Si (284.3 eV), C-C (285.3 eV) and C-N (285.8 eV) [6-8, 9]. The binding energy 284.5eV corresponds to a carbon atom bound only to silicon atom. C-Si bond found due to the reaction between silanol groups of silica coated MION and 3-aminopropyltetraethylorthosilicate. Binding energy 285.3 ascribes to a carbon atom bound only to other carbon atoms and/or hydrogen atoms. 285.8eV corresponds to a carbon bound to single nitrogen atom. This is due to the terminal amino group linked with methylene group. After acrylation, there is significant changes appeared at the peak position and therefore now the peaks can be deconvoluted into six components which are assigned to C-Si (284.3 eV), C=C (284.6 eV), C-C (285.4 eV), N-C=O (286.6 eV), C=O (288 eV) and O-C=O (289.3 eV) [10, 11]. An additional peak found at 284.6eV compare to aminated MION which ascribes the presence of C=C and it is the proof of the acrylation of the aminated MION. Another evidence for this is to the binding energy at 286.6eV for N-C=O which is mainly for the amide formation. The binding energy 289.3eV is due to the presence of O-C=O. This is most probably due to the presence of unreacted methacrylic anhydride. In nanocomposite C1s peak can be deconvoluted into six components peak. The C1s spectrum of nanocomposite shows changing peak position and also peak intensity. With the increasing of binding energy these peaks are assigned to C-Si (284.3 eV), C-C (285.3 eV), C-N (285.8 eV), C-O (286.5 eV), C=O (288 eV), O-C=O (289.3 eV). The peak intensity of C-C is larger compare to another peak. This indicates that the nanocomposite contains greatest C-H or methylene group. The binding energy 286.5eV represents the C-O-C or C-OH bond. This is due to the pyranose ring or alcohol group of the carboxylated cellulose nanocrystals (CCN). Peak position at binding energy 289.3 eV may indicate the presence of carboxylate ion. This is most probably for the poly(acrylic acid) or CCN.

### 3.4.3 High Resolution N1s Spectra

From the widescan spectrum it was seen that N was present but the bonding nature of N with other elements was unknown. The bonding nature of N with other elements high resolution of N1s spectra were carried out. The high resolution N1s spectra of aminated MION, acrylated MION and nanocomposite are shown in figure 3.10.

In the case of aminated MION, there appears one peak at binding energy 400 eV which describes the presence of primary amine at the end of chain. But in the spectra of acrylated

MION there are two deconvoluted peaks appeared. First one is at binding energy 400 eV and second one is for 402 eV. Binding energy 400 eV is attributed to a nitrogen atom linked to a carbon atom by a single bond (amide bond) [12], and the second peak at 402 eV is assigned to the protonated amino group  $\text{-NH}_3^+$  [13]. This indicates that all the amino groups in the aminated MION are not converted to amide. But in the case of nanocomposite there is one peak appeared at 400 eV and indicates the amide group. The protonated amino group which is found in the acrylated MION may be suppressed by the CCN so for it is disappeared in the nanocomposite.

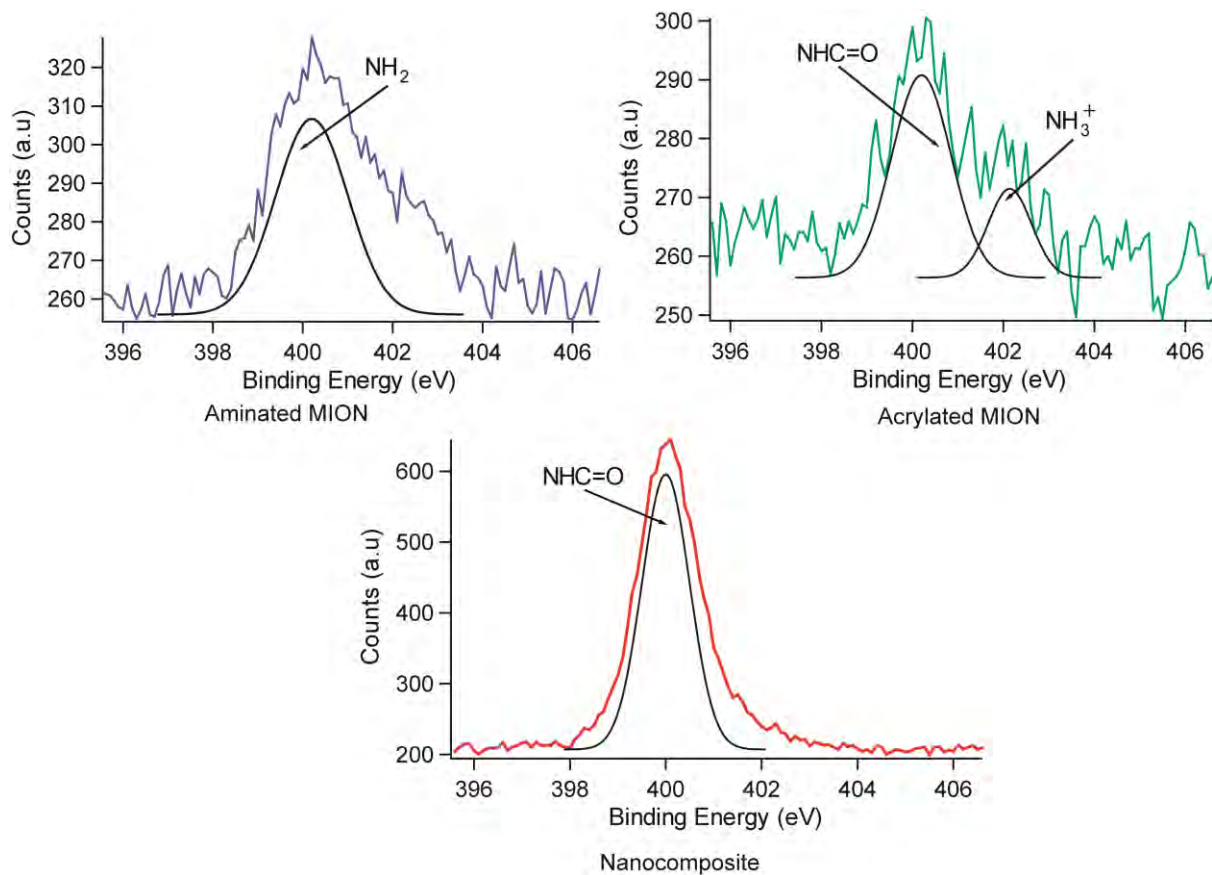


Figure 3.10 High resolution of N1s spectra of aminated MION, acrylated MION and nanocomposite

### 3.5 X-ray diffraction analysis (XRD)

The crystalline properties and phase identification were characterized by X-ray diffraction using a Philips X'pert PRO X-ray diffractometer. The diffractogram was obtained by using Cu-K $\alpha$  radiation ( $\lambda= 0.15406\text{nm}$ ) in the range 10 to 70 °C with steps of 0.021 and acquisition time of 1.0s/step.

The X-ray diffraction patterns of  $\text{Fe}_3\text{O}_4$  and nanocomposite were shown in figure 3.11.

The  $\text{Fe}_3\text{O}_4$  particles have six diffraction peaks at  $2\theta=30.24^\circ$ ,  $35.56^\circ$ ,  $43.38^\circ$ ,  $53.88^\circ$ ,  $57.34^\circ$ , and  $62.82^\circ$ . The peaks are associated with the crystallographic planes or Miller indices of (220), (311), (400), (422), (511), (440) respectively. It can be seen that, the peak position and relative intensities of the diffraction peaks are consistent with the characteristic peaks of standard  $\text{Fe}_3\text{O}_4$  crystal [Joint Committee on Powder Diffraction Standards (JCPDS card No.19-0629)] [14, 15].

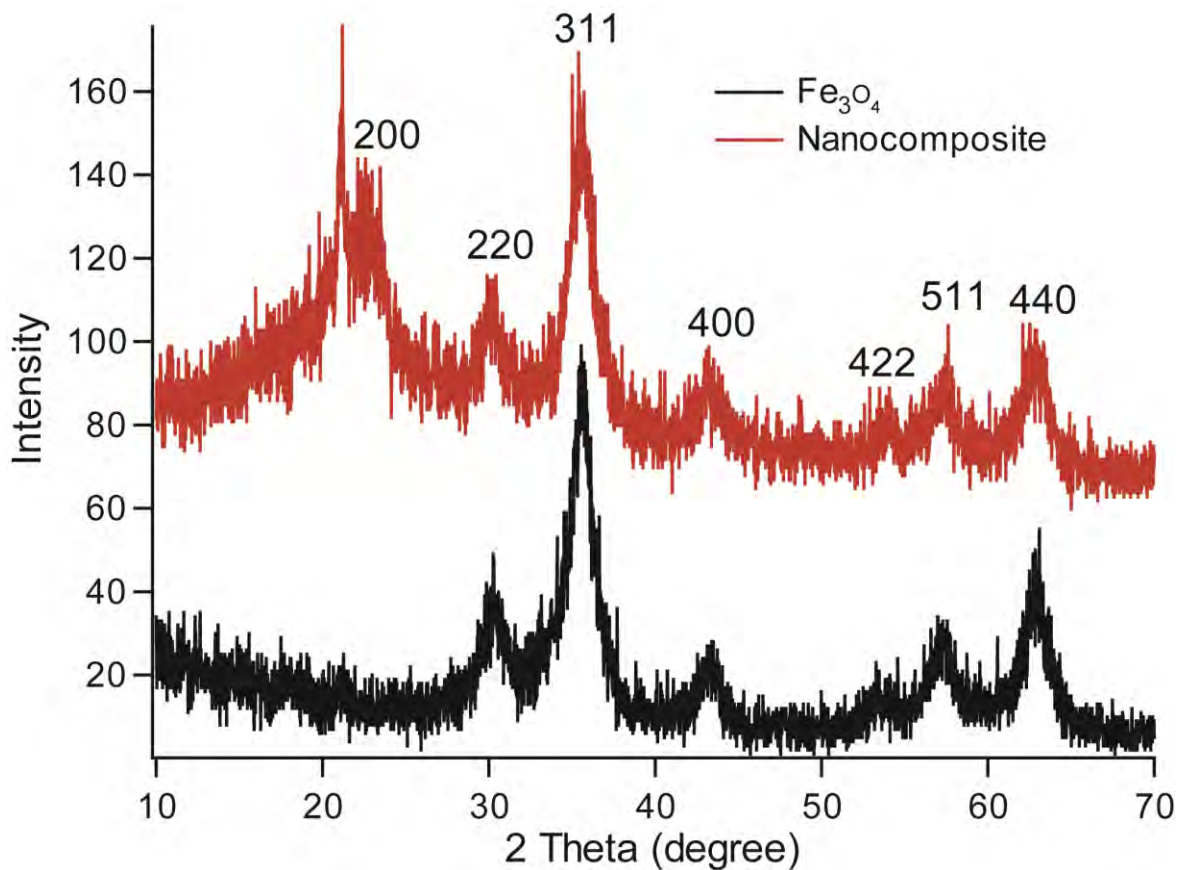


Figure 3.11 XRD spectra of  $\text{Fe}_3\text{O}_4$  and nanocomposite

The diffraction peaks of  $\text{Fe}_3\text{O}_4$  were indexed cubic spinel structure. From XRD data the average crystallite size was determined by Debye-Scherrer equation [16].

$$D_{hkl} = \frac{0.9\lambda}{\beta \cos\theta}$$

Where  $D_{hkl}$  is the average crystallite size,  $\lambda = 0.15406$  nm corresponds to the wavelength of Cu  $K\alpha$  radiation and  $\beta_{hkl}$  is full width half maximum (FWHM) in the  $2\theta$  scale of the diffraction peak from (hkl) crystal planes, and  $\theta$  is the Bragg angle. The crystallite size was determined by taking the average of the sizes at the peaks  $D_{220}$ ,  $D_{311}$ ,  $D_{400}$ ,  $D_{422}$ ,  $D_{511}$  and  $D_{440}$

and it was found to be about 5.32nm. The lattice parameter, “a” was determined by the following equation

$$d_{hkl} = \frac{a}{\sqrt{h^2 + l^2 + k^2}}$$

Where d = interplanar spacing

The lattice parameter was found to be 8.36 Å, which is lower than the values reported JCPDS card No. 19-629(a=8.39), but the value is very close to the theoretical value [17, 18, 19]. The lattice strain was also determined as 0.0237. The 2<sup>nd</sup> XRD pattern is for nanocomposite. From the pattern it is seen that, six peaks of Fe<sub>3</sub>O<sub>4</sub> remained intact although these peaks are a little bit smaller. Moreover, there is a new peak arises at 2θ = 21.2° which is at 200 plane. This peak was found for the CCN. The crystallinity of CCN remained unchanged in the nanocomposite. Broader peak may also be explained as the coating of Fe<sub>3</sub>O<sub>4</sub> with first silica and then functionalized with acrylic group and indicates that crystallinity decreases and amorphous appears. It is also evident that the impurity is present in the nanocomposite.

### 3.6 Surface morphology study using field emission scanning electron microscope (FE-SEM)

Surface morphology of synthesized CNC, CCN, magnetic iron oxide nanoparticles (MION), acrylated MION and nanocomposite was studied by FE-SEM.

The FE-SEM of CNC is shown in figure 3.12.

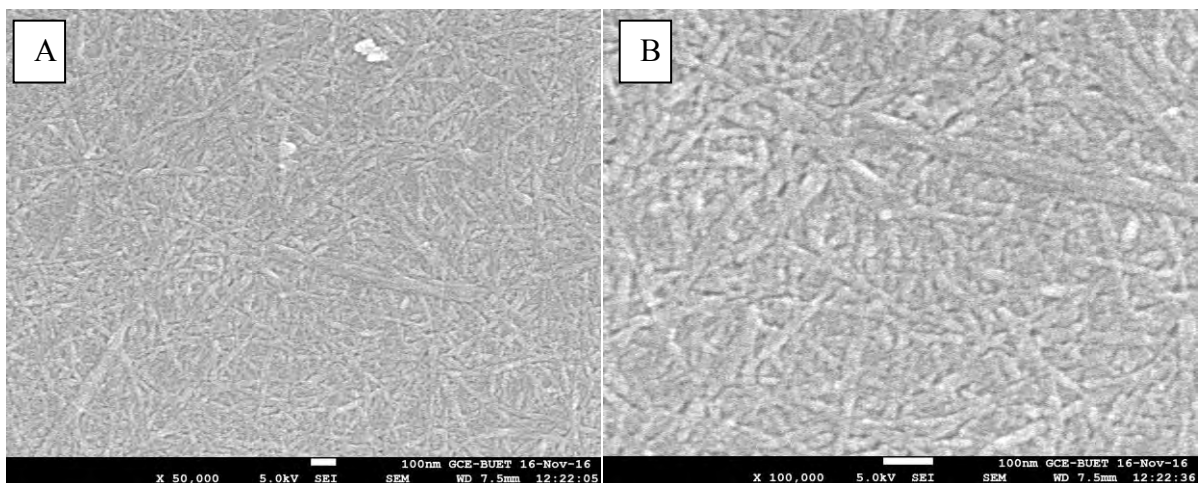


Figure 3.12 SEM image of CNC (A) Resolution x 50,000 (B) Resolution x 100,000

From the figure 3.12, it is seen that CNC are randomly arranged on the film surface and the appearance is like needle shaped. The length of the CNC is about 100-150 nm and diameter is approximately 10-20 nm. As CNC was synthesized by acid hydrolysis process, most of the



amorphous regions are removed resulting the long chain of the cellulose is reduced to a great extent. Due to intermolecular hydrogen bonding CNCs are agglomerate. From both the image at low and high resolution it is seen that the surface is rough.

FE-SEM image of CCN is shown in the figure 3.13.

From the figure 3.13 it is seen that FE-SEM image of CCN is little bit different. The surface is rough and CCNs are randomly arranged. Both low and high resolution images show some white spot.

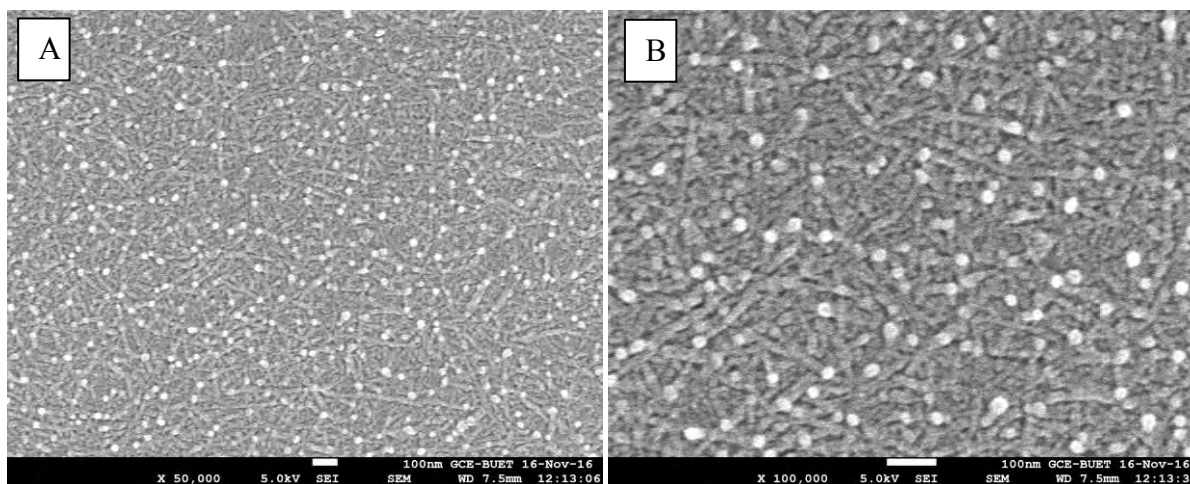


Figure 3.13 FE-SEM image of CCN (A) Resolution x 50,000 (B) Resolution x 100,000.

It is actually spherical CCN which is formed due to concentration variation of TEMPO and sodium hypochlorite. The length of the CCN is about 60-90nm and diameter is approximately 10-20nm. It is also seen that after TEMPO mediated oxidation, the crystal size is little reduced. FE-SEM image of magnetic iron oxide nanoparticle is shown in figure 3.14.

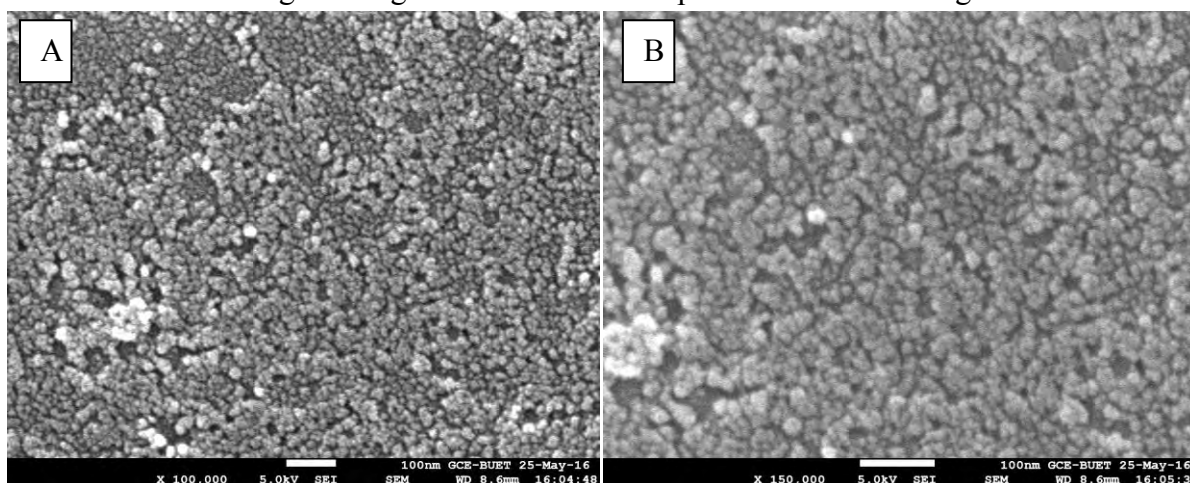


Figure 3.14 FE-SEM image of magnetic iron oxide nanoparticle (MION) (A) Resolution x 100,000 (B) Resolution x 150,000.

From figure 3.14 it is seen that particles of MION are spherical in shape and highly uniform in size. The average particle size is about 10-15nm. Some particles are very small and about 3-5 nm and some particles aggregate due to large surface area and also magnetic attraction among them. From high resolution image it is clearly seen that particles are finely arranged. FE-SEM image of silica coated MION is shown in the figure 3.15.

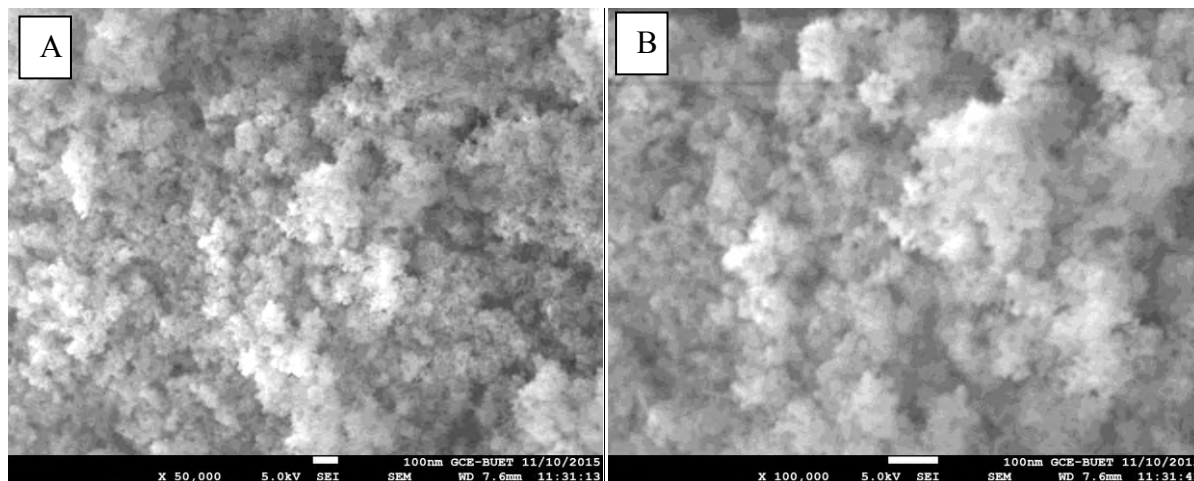


Figure 3.15 FE-SEM image of silica coated MION (A) Resolution x 50,000

(B) Resolution x 100,000.

From the figure 3.15 it is seen that the average size of the silica coated MION is about 15-20 nm.

Surface morphology of acrylated MION was characterized by FE-SEM and the image is shown in figure 3.16.

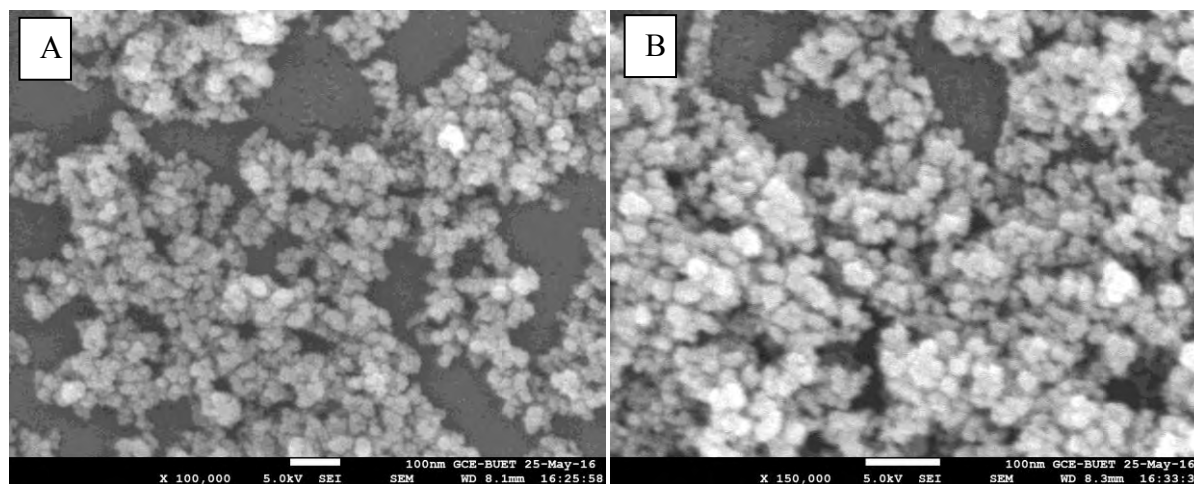


Figure 3.16 FE-SEM image of acrylated MION (A) Resolution x 100,000 (B) Resolution x 150,000.

From the figure 3.16 it is seen that particles of acrylated MION are cubic in shape and size is about 20-30nm. Particles are in randomly arranged and also seen that they are on one another.

The shape of the particles is all most similar which are seen from the high resolution image.

FE-SEM image of nanocomposite is shown in figure 3.17.

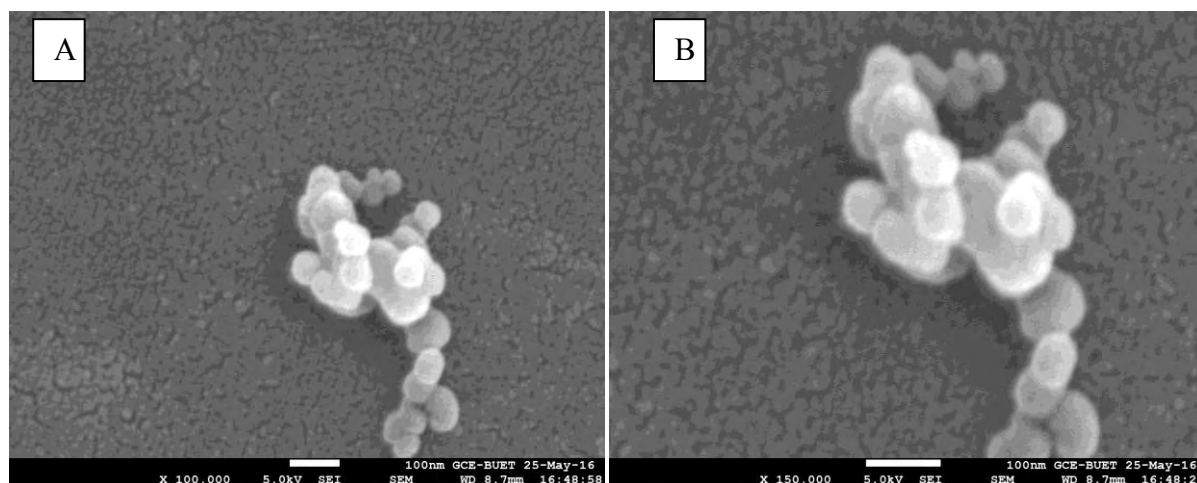


Figure 3.17 FE-SEM image of nanocomposite (A) Resolution x 100,000

(B) Resolution x 150,000

Figure 3.17 shows that the particles of nanocomposite are spherical and the diameter is about 60-90nm. The particles are on one another.

### 3.7 Energy dispersive x-ray spectral analysis

Elemental analyses of the CNC, CCN,  $\text{Fe}_3\text{O}_4$ , silica coated MION, acrylated MION and nanocomposite have been performed by Energy Dispersive X-ray (EDX) method. The EDX patterns are presented in figure 3.18-3.20. The peaks observed at 0.277, 0.392, 0.525, 1.739 and 6.398 keV, for K lines of C, N, O, Si and Fe respectively. The percentages of Fe, O, Si, N, and C were determined from the intensity of the lines and are summarized in Table 3.2.

Table 3.2 Elemental composition of magnetic and cellulosic compound

Sample	Iron (Fe) %	Oxygen (O) %	Silicon (Si)%	Nitrogen (N)%	Carbon (C)%
$\text{Fe}_3\text{O}_4$ (MION)	31	69	×	×	×
Silica coated MION	13	42	43	×	×
Acrylated MION	25	40	12	4	19
CNC	×	52	×	×	47
CCN	×	56	×	×	44
Nanocomposite	1	56	31	1	11



From the table 3.2 it is seen that iron content 31% and oxygen content 69%. It is approximately equal to the theoretical value of  $\text{Fe}_3\text{O}_4$ . In case of CNC, there is some sulfur as the acid hydrolysis was carried out by sulfuric acid and it may form sulfate ester group.

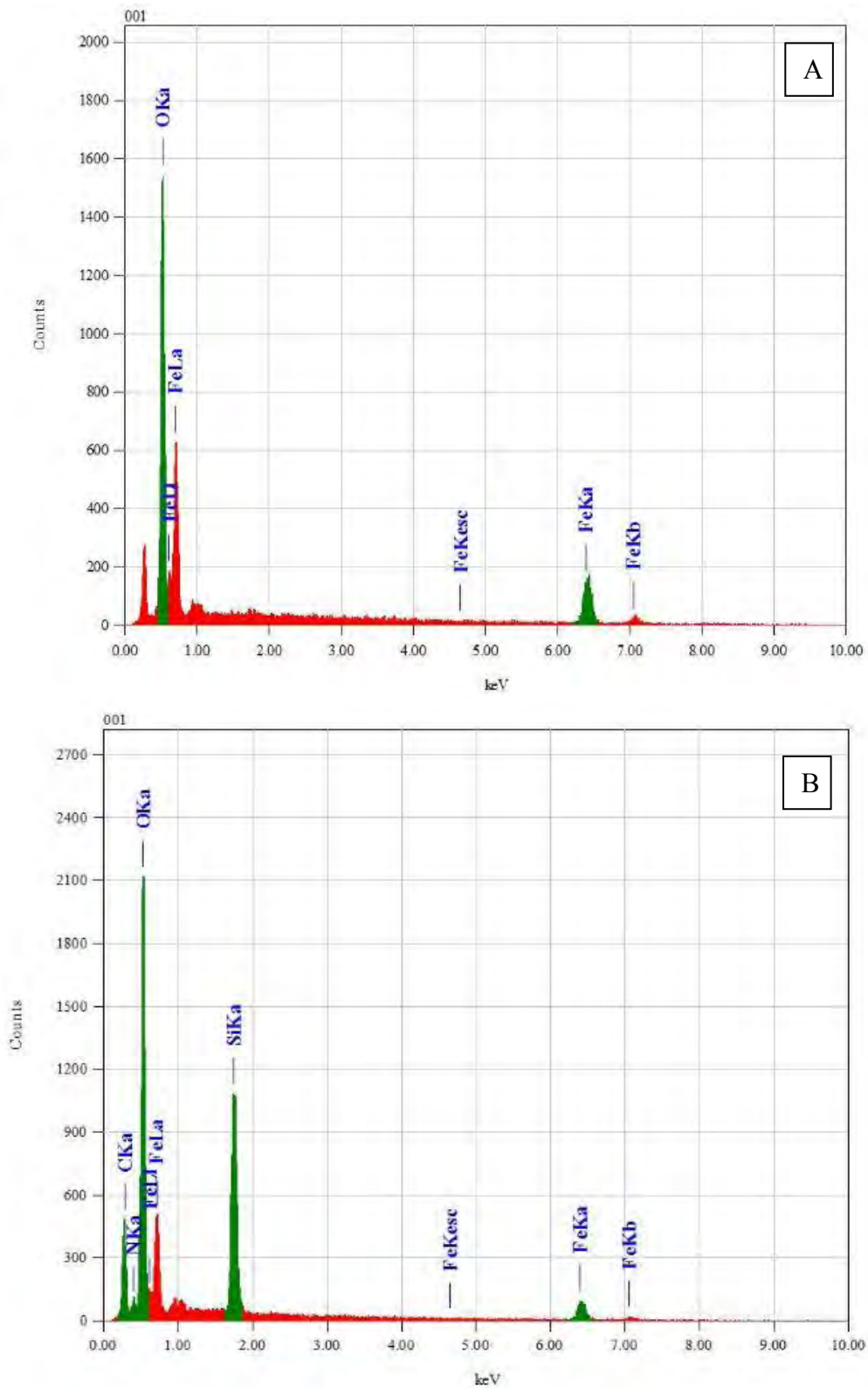


Figure 3.18 EDX spectra of (A)  $\text{Fe}_3\text{O}_4$  (MION) and (B) silica coated MION

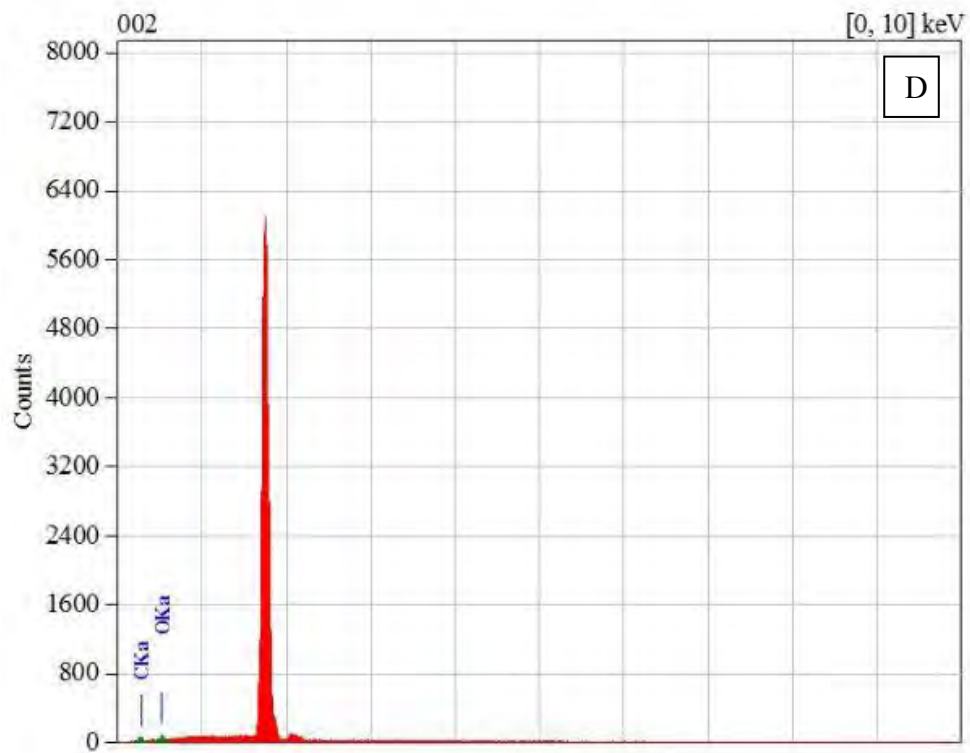
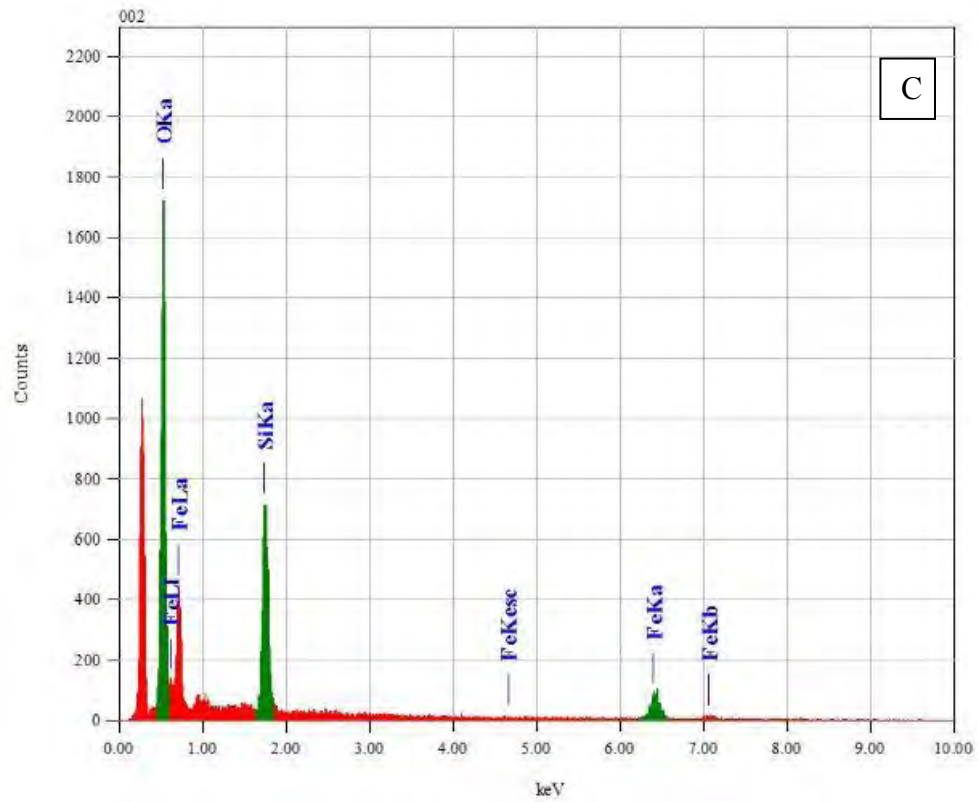


Figure 3.19 EDX spectra of (C) acrylated MION and (D) CNC

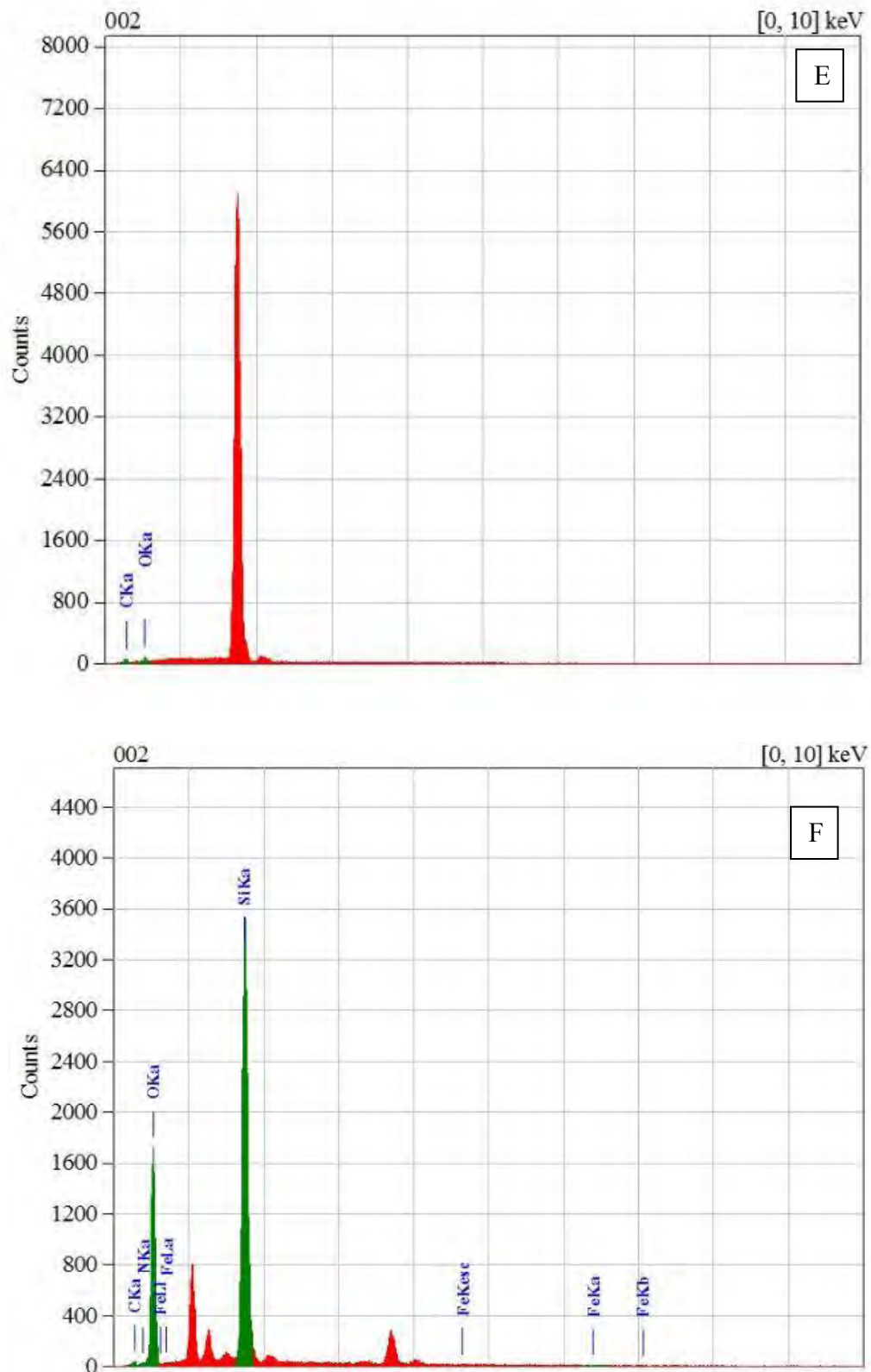


Figure 3.20 EDX spectra of (E) CCN and (F) nanocomposite

### 3.8 Thermogravimetric analysis

Thermal analysis technique such as thermogravimetric analysis was carried out to measure the thermal stability and pyrolysis behavior of CCN, acrylated MION, composite without CCN and nanocomposite at the temperature range 20-800 °C. The TGA curves of CCN, acrylated MION, composite without CCN and nanocomposite are shown in figure 3.21.

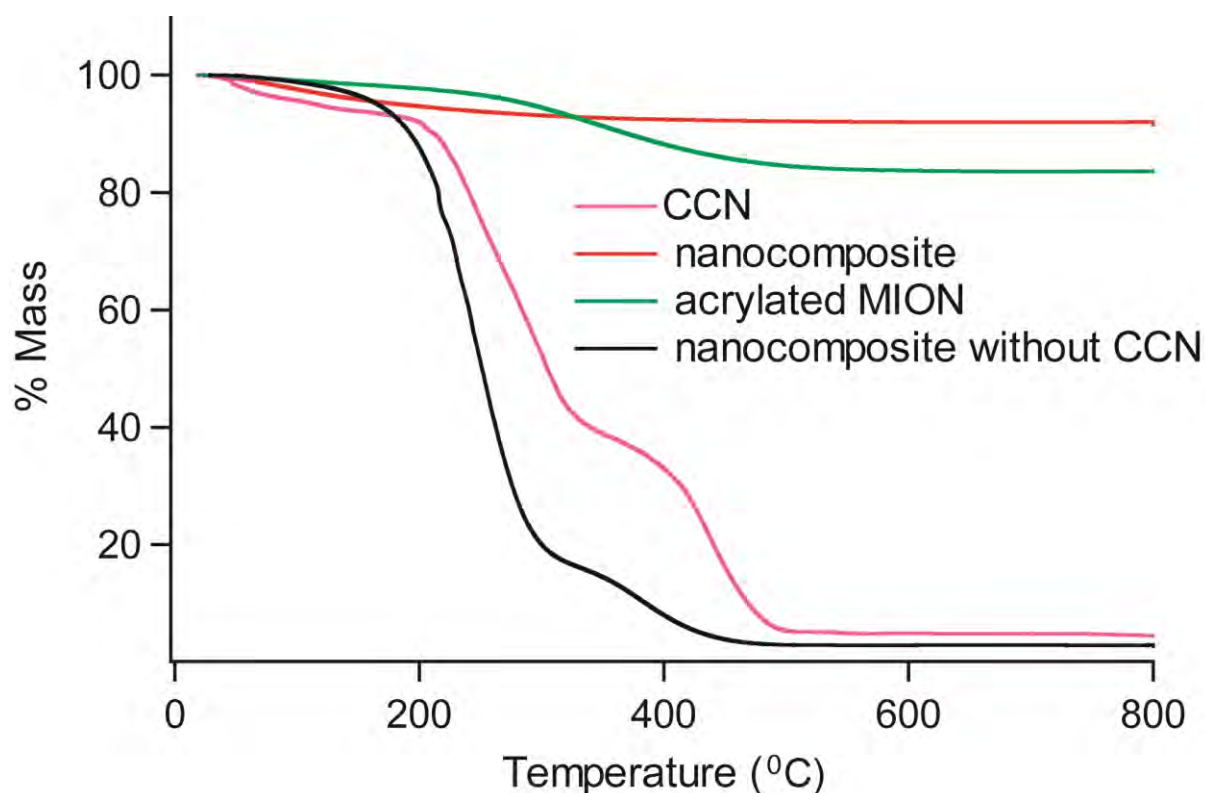


Figure 3.21 TGA curves of CCN, acrylated MION, composite without CCN and nanocomposite

From the TGA curve, it is seen that all the samples showed a slight weight loss at low temperatures ( $< 150$  °C), which is due to the release of water molecules weakly adsorbed on the particles surface. It is also noticed that the degradation behavior was different in the high temperature range. In case of CCN, the initial degradation temperature starts up to  $204$  °C (8.56%). A drastic change appears up to  $330$  °C due to oxygen containing groups disappeared and about 59% weight loss occurred. The final degradation temperature of CCN is  $406$  °C. After  $400$  °C only residue of carbon remained. In case of acrylated MION, the initial degradation temperature is  $257$  °C. With the increasing temperature up to  $483$  °C, oxygen containing group degraded and about 15% weight lost. Next the temperature up to  $800$  °C there is slightly weight change appeared because silica and iron remain unchanged at high

temperature. In case of composite without CCN (3D crosslinked poly(acrylic) acid), the initial degradation temperature is 185 °C. Maximum weight lost occurred at temperature 297 °C which is attributed to the decomposition of the crosslinked polymer network. About 80% weight lost occurred at this temperature. Next weight lost attributed to the oxygen containing groups disappeared. This composite is thermally less stable compared to CCN and acrylated MION. But in the case of nanocomposite, the initial degradation temperature is 216 °C. At this stage about 6% weight lost occurred due to the removal of moisture and adsorbed water. Mechanical strength of nanocomposite was increased due to the incorporation of CCN and dramatically changed its thermal sensitivity. Temperature up to 450 °C only 2% weight lost happened and after that weight remained almost same. So compare to 3D crosslinked poly(acrylic acid) composite and corresponding components, we can say the synthesized nanocomposite is highly thermo stable.

### 3.9 Conclusion

In this study a novel magnetic nanocomposite was synthesized by using 3D crosslinked poly(acrylic acid) and carboxylated cellulose nanocrystals. The 3D crosslinker contains magnetic nanoparticles and are covalently bonded with polymer chains. This nanocomposite when used as adsorbent then its separation becomes very easy. Functional groups of the nanocomposite were analyzed with the help of FTIR study. The surface morphology of the synthesized nanocomposite was characterized by field emission scanning electron microscopy (FE-SEM). From the FE-SEM image it is clear that the size of the particles of the nanocomposite is in nanoscale dimension and also found that particle is about uniform in size. The elemental composition and of the nanocomposite was characterized by x-ray photoelectron spectroscopy (XPS) and energy dispersive x-ray (EDX) analysis. The results show that the successful functionalization of acrylic group in aminated magnetic iron oxide nanoparticles. The XPS results ascribes successful amide bond formation between the amino group of aminated MION and anhydride group of the methacrylic anhydride and confirms the formation of 3D crosslinker. High resolution C1s spectra also confirm the successful incorporation of CCN to the 3D crosslinked poly(acrylic acid) networks. The crystallinity of the nanocomposite was characterized by x-ray diffraction (XRD) analysis. Thermo sensitivity was analyzed by thermogravimetric analysis (TGA). The results show that after the incorporation of CCN into the 3D crosslinked poly(acrylic acid) networks, the thermal stability of the nanocomposite dramatically increased. This indicates that the nanocomposite is highly thermo stable.

## References

1. Kumar, A.; Negi, Y. S.; Choudhary, V.; Bhardwaj, N. K.; “Characterization of cellulose nanocrystals produced by acid-hydrolysis from sugarcane bagasse as agro-waste”, *J. Mater. Physic. Chem.*, vol. 2 (1), pp. 1-8, 2014.
2. de Mesquita, J. P.; Donnici, C. L.; Pereira, F. V.; “Biobased nanocomposites from layer-by-layer assembly of cellulose nanowhiskers with chitosan”, *Biomacromole.*, vol. 11, pp. 473–480, 2010.
3. Gu, J.; Catchmark, J. M.; Kaiser, E. Q.; Archibald, D. D.; “Quantification of cellulose nanowhiskers sulfate esterification levels”, *Carbohydr. Polym.*, vol. 92, pp. 1809–1816, 2013.
4. Azzam, F.; Heux, L.; Putaux, J.; Jean, B.; “Preparation by grafting onto, characterization, and properties of thermally responsive polymer-decorated cellulose nanocrystals”, *Biomacromol.*, vol. 11, pp. 3652–3659, 2010.
5. Xu, J.; Ju, C.; Sheng, J.; Wang, F.; Zhang, Q.; Sun, G.; Sun, M.; “Synthesis and characterization of magnetic nanoparticles and its application in lipase immobilization”, *Bull. Korean Chem. Soc.*, vol. 34, pp. 8, 2013.
6. Diaz, J.; Paolicelli, G.; Ferrer, S.; Comin, F.; “Separation of the sp<sup>3</sup> and sp<sup>2</sup> components in the C1s photoemission spectra of amorphous carbon films”, *Phys. Rev. B.*, vol. 54, pp. 8064- 8069, 1996.
7. Li, Q. X.; Wen, J. Y.; Neoh, K. G.; Kang, E. T.; Guo, D. F.; “Dopamine-induced reduction and functionalization of graphene oxide nanosheets”, *Macromole.*, vol. 43, pp. 8336-8339, 2010.
8. Gao, H. C.; Sun, Y. M.; Zhou, J. J.; R. X.; Duan, H. W.; “Mussel-inspired synthesis of polydopamine-functionalized graphene hydrogel as reusable adsorbents for water purification”, *Acs Appl. Mater. Interfaces*, vol. 5, pp. 425-432, 2013.
9. Bashouti, M. Y.; Garzuzi, C. A.; de la Mata, M.; Arbiol, J.; Ristein, J.; Haick, H.; Christiansen, S.; “Role of Silicon Nanowire Diameter for Alkyl (Chain Lengths C1–C18) Passivation Efficiency through Si–C Bonds”, *Langmuir*, vol. 31, pp. 2430–2437, 2015.

10. Liu, F.; Sun, F.; Pan, Q.; “Highly compressible and stretchable superhydrophobic coating inspired by bio-adhesion of marine mussels”, *J. Mater. Chem., A*, vol. 2, pp. 11365-11371, 2014.
11. Barazzouk, S.; Daneault, C.; “Amino acid and peptide immobilization on oxidized nanocellulose: spectroscopic characterization”, *Nanomaterials*, vol. 2, pp. 187-205, 2012.
12. Jansen, R. J. J.; Van Bekkum, H.; “XPS of nitrogen-containing functional groups on activated carbon”, *Carbon*, vol. 33, pp. 1021–1027, 1995.
13. Zubavichus, Y.; Zharnikov, M.; Shaporenko, A.; Fuchs, O.; Weinhardt, L.; Heske, C.; Umbach, E.; Denlinger, J.D.; Grunze, M.; “Soft X-ray induced decomposition of phenylalanine and tyrosine: A comparative study”, *J. Phys. Chem. A*, vol. 108, pp. 4557–4565, 2004.
14. He, Y. P.; Wang, S. Q.; Li, C. R.; Miao, Y. M.; Wu, Z. Y.; Zou, B. S.; “Synthesis and characterization of functionalized silica-coated Fe<sub>3</sub>O<sub>4</sub> superparamagnetic nanocrystals for biological applications”, *J. Phys. D: Appl. Phys.* vol. 38, pp. 1342–1350, 2005.
15. Zhang, H.; Zhong, X.; Xu, J. J.; Chen, H. Y.; “Fe<sub>3</sub>O<sub>4</sub>/Polypyrrole/Au nanocomposites with core/shell/shell structure: synthesis, characterization, and their electrochemical properties”, *Langmuir*, vol. 24, pp. 13748-13752, 2008.
16. Fang, M.; Strom, V.; Olsson, R. T.; Belova, L.; Rao, K. V.; “Particle size and magnetic properties dependence on growth temperature for rapid mixed co-precipitated magnetite nanoparticles”, *Nanotech.*, vol. 23, pp. 145601, 2012.
17. Wu, W.; Xiao, X.; Zhang, S.; Zhou, J.; Fan, L.; Ren, F.; Jiang, C.; “Large-Scale and Controlled Synthesis of Iron Oxide Magnetic Short Nanotubes: Shape Evolution, Growth Mechanism, and Magnetic Properties”, *J. Phys. Chem. C*, vol. 114, pp. 16092-16103, 2010.
18. Iwasaki, T.; Nami Sato, N.; Kosaka, K.; Watano, S.; Yanagida, T.; Kawai, T.; “Direct transformation from goethite to magnetite nanoparticles by mechanochemical reduction”, *J. Alloy. Compd.*, vol. 509(4), pp. L34–L37, 2011.



19. Vaidyanathan, G.; Sendhilnathan, S.; Arulmurugan, R.; “Structural and magnetic properties of  $\text{Co}_{1-x}\text{Zn}_x\text{Fe}_2\text{O}_4$  nanoparticles by co-precipitation method,” *J. Magn. Mater.*, vol. 313, pp. 293 – 299, 2007.